Epilepsy-linked kinase CDKL5 phosphorylates voltage-gated calcium channel Cav2.3, altering inactivation kinetics and neuronal excitability

Marisol Sampedro-Castañeda[1,5]*, Lucas L Baltussen[1,4,5], Andre T Lopes[1], Yichen Qiu[2], Liina Sirvio[1], Simeon R. Mihaylov[1], Suzanne Claxton[1], Jill C Richardson[3], Gabriele Lignani[2], Sila K Ultanir[1]*

1. Kinases and Brain Development Lab, The Francis Crick Institute, 1 Midland Road, London NW1 1AT, United Kingdom

2. Department of Clinical and Experimental Epilepsy, UCL Queen Square Institute of Neurology, 808 Queen Square House, London WC1N 3BG, United Kingdom

3. UK Neuroscience Group, MSD R&D Innovation Centre, 120 Moorgate, London, EC2M 6UR, United Kingdom

*Correspondence: sila.ultanir@crick.ac.uk

marisol.sampedro-castaneda@crick.ac.uk

4. Current address: Laboratory of Synapse Biology (VIB-KU Leuven), Department of Neurosciences, ON5 Herestraat 49, 3000 Leuven, Belgium

5. These authors contributed equally

SUMMARY

Developmental and epileptic encephalopathies (DEEs) are a group of rare childhood disorders characterized by severe epilepsy and related cognitive deficits. Numerous DEE genes have been discovered thanks to advances in genomic diagnosis, yet putative molecular links between these disorders are not known. CDKL5 deficiency disorder (CDD, DEE2) is one of the most common forms of genetic epilepsy; it is caused by loss-of-function mutations in the brain-enriched kinase CDKL5. To elucidate CDKL5 function, we looked for CDKL5 substrates using a SILAC based phosphoproteomic screen. We identified the voltage-gated Ca^{2+} channel Cav2.3 (encoded by *CACNA1E*) as a novel physiological target of CDKL5 in mice and humans. Recombinant channel electrophysiology and interdisciplinary characterization of Cav2.3 phosphomutant mice revealed that the loss of Cav2.3 phosphorylation leads to channel gain-of-function via slower channel inactivation and enhanced acetylcholine-induced stimulation, resulting in increased neuronal excitability. These changes in Cav2.3 closely resemble those described for gain-of-function point-mutations in *CACNA1E* that cause DEE69, a disorder sharing clinical features with CDD. Our results show that these two single-gene disorders are mechanistically related. We suggest that CDD is partly a channelopathy with Cav2.3 gain-of-function, thus Cav2.3 inhibition could be therapeutic in these DEEs.

KEYWORDS

CDKL5, CACNA1E, Cav2.3, epilepsy, developmental and epileptic encephalopathy, DEE2, DEE69

HIGHLIGHTS

- CDKL5 phosphorylates Cav2.3 at Ser15 and reduces channel inactivation time
- Loss of CDKL5 causes Cav2.3 gain-of-function, mimicking pathological *CACNA1E* mutations
- Hippocampal neurons from Cav2.3 S15A mutant mice have an enhanced excitability response to cholinergic stimulation
- A common molecular mechanism connects CDKL5 and *CACNA1E* epileptic encephalopathies

INTRODUCTION

Developmental and epileptic encephalopathies (DEE) are characterized by severe early-onset epileptic activity accompanied by global developmental and cognitive impairments. The genetic aetiology for 100 DEEs have been identified, but targeted therapies remain scarce. Elucidating shared pathways in infantile-onset epilepsies will reveal molecular links between disease genes and greatly advance common targeted treatments.

Cyclin dependent kinase like-5 (CDKL5) is a brain-enriched serine-threonine kinase. *De novo* loss-of-function mutations in the X-linked *CDKL5* gene, including missense, nonsense and insertions/deletions, cause CDKL5 deficiency disorder (CDD) (OMIM 300672, 300203) [1-4]. Pathogenic missense mutations, almost exclusively located in the kinase domain, indicate that kinase activity is critical for CDD pathology [5-8]. CDD is characterized by infantile-onset, intractable seizures, profound neurodevelopmental impairment in motor and sensory function, impaired language acquisition and autonomic disturbances [2, 4]. The estimated incidence for CDD is 1/42,000 live births each year [9-11] with approximately 80% female patients, making it the second most common type of genetic childhood epilepsy [12, 13].

CDKL5 is highly enriched throughout the forebrain with expression starting at late embryonic stages in rodents and humans [14-18]. Low levels of expression were reported in other tissues [15]. Phosphorylation targets include microtubule binding proteins EB2 and MAP1S [5, 19] and transcriptional regulators ELOA [20] and Sox9 [21], showing its diverse cellular roles. CDKL5 KO mouse neurons have deficits in synaptic transmission, dendritic spine development, neurite outgrowth, cilia elongation and microtubule dynamics [22-27]. However, molecular mechanisms linking CDKL5 loss to neuronal hyperexcitability remain unknown. The identification of key physiological targets of CDKL5 directly involved in the regulation of cellular excitability may help elucidate epileptogenic mechanisms and lead to targeted therapies.

Voltage-gated calcium channels (VGCC) have a key role in physiology, driving neuronal excitability and allowing influx of second messenger Ca^{2+} ions in response to membrane depolarization [28-30]. VGCC subtype Cav2.3 is formed by the ion-conducting α1E subunit (encoded by *CACNA1E*) in complex with accessory subunits from the β and α2δ families. Cav2.3 is highly expressed in the CNS, where it is localized at both pre- and post-synaptic sites in neurons, as shown functionally and by immuno-EM [31-33]. *CACNA1E* knockout mice demonstrated that Cav2.3 mediates neuronal R-type Ca^{+2} currents [33-35], so-called due to their "resistance" to organic VGCC channel inhibitors [36, 37]. Cav2.3 is dynamically regulated by phosphorylation at multiple sites [38, 39]. In general, VGCC phosphorylation is an important mechanism by which neuromodulators and their G-protein coupled receptors (GPCRs) exert their effect on cellular excitability [40].

101 *De novo* heterozygous missense mutations in *CACNA1E* cause an infantile epileptic
102 encephalopathy (OMIM 618285) [41, 42]. Cav2.3 variants studied *in vitro* have altered gating
103 and/or inactivation kinetics, leading to gain-of-function (GoF) of Cav2.3 [41, 42]. Patients with
104 *CACNA1E* mutations have overlapping clinical phenotypes with CDD, such as intractable
105 seizures, profound intellectual disability and hypotonia. Single-gene DEEs such as this one
106 are estimated to impact approximately 1/2100 live births [9], but their real prevalence is unknown
107 as more genes are being identified rapidly due to recent advances in genetic diagnosis [43, 44].
108 Despite, overlapping clinical features, potential molecular links between each of these rare
109 disorders remain to be elucidated.
110
111 In this work, we apply for the first time a global phosphoproteomics approach in CDKL5
112 knockout mice and identify and validate Cav2.3 as a novel substrate of CDKL5 in human and
113 mouse neurons. Through our analysis of Cav2.3 function and characterization of a novel
114 Cav2.3 phosphomutant mouse line, in which CDKL5 phosphorylation site is mutated, we
115 reveal that lack of phosphorylation leads to Cav2.3 gain-of-function and hyperexcitability. Our
116 results indicate that developmental and epileptic encephalopathies caused by *CDKL5* and
117 *CACNA1E* are related at the molecular level. We propose Cav2.3 as a converging therapeutic
118 target for these disorders.
119
120

121 **RESULTS**

122 **Cav2.3 is a CDKL5 phosphorylation substrate in mice and humans**

123 We used stable isotope labelling of amino acids in cell culture (SILAC) [45] to differentially tag
124 newly synthesized proteins in primary cortical cultures from wild type (WT) and CDKL5
125 knockout (KO) mice [46] and compare changes in protein phosphorylation levels (Fig. 1a). As
126 expected in CDKL5 KO neurons, we observe a significant reduction in CDKL5 pS407 and in
127 EB2 pS222, a known CDKL5 phosphorylation target [19]. Phosphorylation of EB2 S221 was
128 also decreased, indicating co-regulation of these neighbouring sites. More importantly, a
129 potential new target protein, the ion channel Cav2.3, showed strongly reduced
130 phosphorylation at S15 (pS15), in CDKL5 KO neurons. Strikingly, the Cav2.3 S15 site matches
131 the RPXS/T* consensus motif [5, 19], suggesting direct CDKL5 phosphorylation (Fig. 1a, b). S15,
132 located in the N-terminus of the α1E channel pore subunit (Fig. 1b), is conserved in humans
133 (S14) but absent in the related Cav2.1 (*CACNA1A*) and Cav2.2 (*CACNA1B*) channels (Fig.
134 1b).

135 To test if CDKL5 can phosphorylate Cav2.3 S15, we generated a phosphospecific antibody
136 targeting this site. Overexpression of Cav2.3 (& ancillary subunits) together with the CDKL5

kinase domain in HEK293 cells shows strong Cav2.3 phosphorylation *in vitro* (Cav2.3 pS14, Fig. 1c, f). This phosphorylation is absent when overexpressing phosphomutant Cav2.3 or kinase-dead CDKL5, demonstrating the specificity of the antibody and the dependence of phosphorylation at this site on CDKL5 kinase activity. Importantly, full-length CDKL5 also directly phosphorylated Cav2.3 *in vitro* (Fig. S1a, b). Cav2.3 phosphorylation is consistently reduced in the cortex of CDKL5 KO mice at postnatal day P20 (Cav2.3 pS15), validating the substrate *in vivo* (Fig. 1d, g). Finally, Cav2.3 pS14 was decreased in human iPSC-derived neurons from CDD patients (Fig. 1e, h), demonstrating altered phospho-regulation of this target in CDD. Together, these results show that Cav2.3 is a *bona fide* CDKL5 phosphorylation target in mice and humans.

Loss of Cav2.3 Ser14 phosphorylation slows baseline channel kinetics and amplifies muscarinic regulation

Cav2.3 is causally linked to epilepsy by two main lines of evidence. First, channel deletion renders mice resistant to tonic-clonic seizures [47-49]. On the other hand, Cav2.3 GoF leads to severe epileptic encephalopathy in humans [41, 42]. The remarkable overlap in clinical manifestations between CACNA1E and CDD patients, including seizures and neurodevelopmental delays, raises the possibility that Cav2.3 regulation by CDKL5 might affect channel function and in turn neuronal excitability.

To test the effect of pS14 on Cav2.3 channel properties we used a HEK293 cell line stably expressing the human auxiliary subunits β3 and α2δ1 and transiently transfected human α1E and full-length CDKL5 plasmids (Fig. S1a, b). Whole-cell patch-clamp recordings of Cav2.3 Ba^{2+} currents revealed slower decay kinetics (inactivation τ) in S14A mutant channels (Fig. 2a-c). Notably, in absence of CDKL5, WT Cav2.3 decay kinetics were indistinguishable from S14A Cav2.3 mutant (Fig. 2d). We also found a statistically significant increase in whole-cell current density at maximum activation voltages in S14A when compared to WT Cav2.3 in presence of CDKL5 (Fig. 2e). To account for differences in biophysical properties that may be introduced by α1E association with a different β subunit [50, 51], we conducted parallel experiments in a HEK293 cell line stably expressing human α2δ1 and β1b, another Cavβ subunit associated with α1E in the brain [52]. We used Ca^{2+} as charge carrier to examine channel properties in a more physiological context. Decay kinetics of WT Cav2.3 currents with β1b were substantially slower than currents with β3 (Fig. S2 a, b *vs.* Fig 1a, b), as previously reported [50]. In absence of CDKL5 phosphorylation (S14A α1E mutant or kinase-dead CDKL5 conditions), Cav2.3 current inactivation was further slowed (Fig. S2a-c), recapitulating our results with β3 (Fig. 2a-c). Current density at maximal activation voltages did not reach significance in the β1-expressing cells, where currents were generally larger (Fig. S2d).

173 Finally, we observed no changes in half maximal activation and inactivation potential or time
174 course of recovery from fast inactivation in β3- or β1-expressing cells (Fig. 2f & S2e,f).

175 Altogether, our results indicate that CDKL5-mediated Ser14 phosphorylation of α1E speeds
176 up the inactivation of human Cav2.3 and suppresses current amplitude, independent of Cavβ
177 subtype or charge carrier. Consequently, absence of CDKL5 leads to Cav2.3 GoF, with larger
178 and more prolonged currents. A subset of *CACNA1E* GoF mutations described in human DEE
179 patients also cause slower inactivation kinetics and/or increased current density [41], mirroring
180 the phenotypes observed in the unphosphorylated channel. Thus, the functional deficits in
181 Cav2.3 observed in absence of CDKL5 phosphorylation match those caused by pathological
182 point mutations in Cav2.3 and could partly explain the pathophysiology of CDD.

183 Cav2.3 channels are downstream targets of muscarinic acetylcholine receptors, which modify
184 channel function predominantly via PKC-mediated phosphorylation, leading to current
185 enhancement in HEK293 cells and neurons [53-55]. Given the observed GoF in S14A Cav2.3,
186 we hypothesized that muscarinic receptor enhancement may also be affected by CDKL5
187 phosphorylation. To test this, we co-expressed Cav2.3, CDKL5 and muscarinic acetylcholine
188 receptor type 3 or 1 (M3 or M1), which are prominent brain subtypes known to regulate
189 neuronal Cav2.3 post-synaptically. As expected, application of the non-hydrolysable agonist
190 carbachol substantially increased current amplitude regardless of Ser14 phosphorylation in
191 both β3 and β1 stable cell lines (Fig. 2g-l). The current increase with carbachol was 1.5- to 2-
192 fold greater in cells without phospho-Ser14 at -10 mV (Fig. 2g, h, j, l), reflecting Cav2.3 gain-
193 of-function in absence of phosphorylation. The half-maximal activation potential ($V_{1/2}$) was left-
194 shifted by 5 mV for WT channels in both cell lines, a described effect of muscarinic receptor
195 activation [54, 56]. Interestingly, without Ser14 phosphorylation this shift was significantly greater,
196 implying an effect of phospho-Ser14 on the modulation of Cav2.3 gating (Fig. 2m-p). This
197 represents an additional gain-of-function due to loss of CDKL5, a phenotype comparable to
198 pathogenic *CACNA1E* mutations that alter $V_{1/2}$ [41].

199 Upon GPCR activation, Cav2.3 channels can be suppressed by $G_{\beta\gamma}$ subunits. This effect is
200 has been observed in Gαq-coupled receptors including M1/M3 in HEK293 cells [54] and CA1
201 neurons [53]. The Cav2.3 N-terminus and Cavβ are involved in $G_{\beta\gamma}$ regulation [57, 58]. For this
202 reason, we investigated the possibility that the enhanced carbachol effects in absence of N-
203 terminal pS14 could be due to reduced $G_{\beta\gamma}$ suppression. To distinguish between PKC-
204 mediated enhancement and $G_{\beta\gamma}$ suppression, we boosted PKC activity prior to carbachol
205 application using phorbol 12-myristate 13-acetate (PMA), reliably increasing Cav2.3 currents
206 [54, 59]. With further addition of carbachol we found no evidence of muscarinic inhibition of human
207 WT Cav2.3 channels (Fig. S2g,h). Moreover, co-expression of Cav2.3 and Gi-coupled
208 dopamine D2 receptors to further probe $G_{\beta\gamma}$ inhibition in our system, revealed significant
209 reduction in peak currents upon D2 activation with quinpirole [57]. However, there was no

210 difference in inhibitory modulation with or without Ser14 phosphorylation (Fig. S2i,j). The
211 above manipulations suggest that $G_{\beta\gamma}$ is not involved in pathological Cav2.3 GoF.

212 Our results describe two Cav2.3 gain-of-function (GoF) mechanisms in the absence of CDKL5
213 phosphorylation: slower decay kinetics and a left shift in voltage-dependence of activation
214 ($V_{1/2}$) upon muscarinic activation, both reflected in increased Ca^{2+} influx through Cav2.3
215 channels. These GoF features are reminiscent of those described for pathological Cav2.3
216 variants.

217

218 **Altered R-type current inactivation and increased excitability in neurons from Cav2.3**
219 **S15A phosphomutant mice**

220 To investigate the role of Cav2.3 S15 phosphorylation in neurons, we generated Cav2.3 S15A
221 phosphomutant mice using CRISPR-Cas9 genome editing. We found that the total S15
222 phosphorylation levels detected by our phosphoantibody were reduced to <20% of control
223 levels in homozygous S15A mice (HOM S15A) while total Cav2.3 levels were not changed
224 (Fig. 3a-c). Cav2.3 is highly expressed in the somato-dendritic region of CA1 hippocampal
225 neurons [32] where it underlies most of the R-type current and regulates intrinsic excitability [33,
226 53]. We performed whole-cell somatic recordings in acute slices from young mice and recorded
227 pharmacologically isolated Cav2.3 Ca^{2+} currents in these cells. When compared to wild type
228 littermates (WT), HOM S15A mice showed significantly slower inactivation τ at maximal
229 conductance voltages, recapitulating HEK293 cell results (Fig. 3 d,e). Current amplitudes at
230 the soma did not differ (Fig. 3f).

231 We next tested the effect of Cav2.3 S15A on neuronal excitability and cholinergic
232 neuromodulation in response to depolarising current injections in adult CA1 pyramidal cells.
233 Resting membrane potential (V_{rest}), input resistance (R_{in}) and firing properties were identical
234 between WT and S15A mice under baseline conditions (Fig. 3g-i). Following bath application
235 of carbachol, we observed a 4mV depolarisation in V_{rest} and a 25% increase in R_{in} (Fig 3g),
236 changes that were comparable between WT and S15A neurons (Fig. S3a). These alterations
237 are likely due to conductances other than Cav2.3, in line with previous reports [56, 60, 61].

238 In neurons, cholinergic activation can elicit sustained depolarizing plateau potentials (DPPs):
239 all-or-none, large amplitude depolarizations that outlast stimulus-evoked firing [56, 62, 63]. A
240 muscarinic medium duration afterdepolarization (ADP) is also reported in CA1 pyramidal cells
241 [64]. Up-regulation of Cav2.3-mediated R-type currents is required for DPPs and ADPs in
242 hippocampus [65] and cortex [63]. We inspected these Cav2.3-dependent hyper-excitability
243 measures in S15A mice. Carbachol application significantly increased action potential firing
244 frequency in WT and S15A neurons (Fig. 3 h-k). At current injections greater than 250 pA,

245 however, phosphomutant neurons responded with fewer spikes and depolarization block
246 towards the end of the stimulus step, indicating greater underlying depolarization. The
247 percentage of cells exhibiting at least one DPP or all-or-none afterdepolarization (ADP) >8 mV
248 upon carbachol treatment was significantly higher in S15A mice, showing an enhanced
249 depolarization response (Fig. 3j, k). Importantly, the occurrence of DPP/large ADPs was
250 shifted towards lower current injections in S15A cells (Fig. 3l). Greater perisomatic
251 depolarization in S15A neurons was also reflected in a larger ADP at 100ms post stimulus and
252 more spike attenuation (Fig. S3b, c). Together with the enhanced carbachol-mediated left-
253 shift in $V_{1/2}$ observed in phosphomutant channels in HEK293 cells (Fig. 2 j,l), these increased
254 neuronal depolarizations in Cav2.3 phosphomutant mice suggest facilitation of gating of
255 endogenous Cav2.3 without S15 phosphorylation upon cholinergic agonist application.

256 We tested if other conductances known to be regulated by carbachol are altered in Cav2.3
257 phosphomutants. The medium- and slow-afterhyperpolarizations (AHPs) are critical for spike
258 frequency regulation and their underlying K^+ and mixed-cationic currents are targets of the
259 muscarinic system [60, 66, 67]. Baseline AHPs elicited by a short spike burst were not different
260 between WT and S15A mice and were equally suppressed by carbachol application (Fig. S3d).
261 We also analysed baseline small-conductance Ca^{2+}-activated K^+ (SK) currents and
262 spontaneous excitatory synaptic currents (EPSCs), known to be functionally coupled to [68] or
263 modulated by [69] Cav2.3 in CA1 neurons. We hypothesized that these may be affected given
264 the prolonged Cav2.3 currents in S15A mice, but our measurements show no differences
265 between genotypes (Fig. S3e-h). Therefore, we suggest that the increased carbachol-induced
266 excitability of CA1 neurons in Cav2.3 S15A knock-in mice is specifically due to Cav2.3 GoF.

267

268 **Cav2.3 S15A phosphomutant mice have behavioural and EEG deficits**

269 Multiple CDKL5 KO mouse models have been generated [14, 17, 46] by deleting exons 4, 2 or 6,
270 all of which lead to loss of CDKL5 protein. Several behavioural deficits were reported in these
271 mice [46, 70, 71]. We investigated behavioural phenotypes in Cav2.3 S15A phosphomutant mice
272 and tested if they recapitulate reported CDKL5 KO impairments. Initially, we observed no overt
273 behavioural alterations or spontaneous seizures, as reported for CDKL5 KO mice [14, 17, 72], but
274 see [73, 74]. However, when monitored in a home-cage environment for prolonged periods, S15A
275 showed reduced locomotion and voluntary wheel use (Fig. 4a, b), prompting closer
276 behavioural examination. We observed minor changes in locomotion and zone preference in
277 the open field test, but only towards the end of a 30 min trial (Fig. 4c, S4a), potentially
278 indicating fatigue rather than anxiety. Unlike CDKL5 KOs, S15A mice did not present hindlimb
279 clasping (mean scores: WT 0.041, HOM S15A 0, p=0.334, unpaired t test) and performed
280 equally in the rotarod test (Fig. 4d) when compared to WT littermates. Cognitive abilities in the

281 Y- and Barnes maze were also unchanged in phosphomutants (Fig. S4b-e). On the other
282 hand, S15A mice had mild impairments in sociability (Fig. 4e). A consistently reported
283 phenotype of CDKL5 KO mice is altered contextual fear conditioning responses [14, 71].
284 Strikingly, memory formation, retention and extinction in this task were also defective in Cav2.3
285 S15A (Fig. 4f), indicating a clear overlap with CDKL5 KOs.

286 Finally, given the high epilepsy incidence in human CDKL5 and CACNA1E DEE patients,
287 seizure susceptibility was analysed in a separate cohort using wireless electrocorticogram
288 (ECoG) transmitters [75] and repeated low-dose kainic-acid (KA) injections [76] (Fig. 4g-i). We
289 found no changes in baseline ECoG (Fig 4g) or overall KA-induced seizure susceptibility in
290 S15A mice (Fig. 4h), as reported for CDKL5 KO mouse models [17, 35]. Interestingly, however,
291 female phosphomutant mice had a reduced threshold to stage 5 behavioural seizures with an
292 increase in ECoG activity during KA (Fig. 4h,i).

293 In summary, our *in vivo* analyses of S15A mutant mice demonstrate similarities with CDD
294 mouse models and patients, including social, motor and cognitive impairments, and to some
295 extent increased seizure susceptibility. These observations suggest that loss of pS15 is a key
296 contributor to the phenotypic features of CDD.

297

298 **DISCUSSION**

299 There are currently no disease-targeting therapies for CDD and the causes of aberrant
300 excitability in absence of CDKL5 are unknown. Here we identify the alpha subunit of Cav2.3
301 channel complex as a CDKL5 phosphorylation substrate in mouse and human neurons.
302 *CACNA1E* mutations cause severe early onset epilepsy in humans and there is remarkable
303 overlap between CDD and patients with *CACNA1E* mutations. These include intractable
304 seizures, global developmental delay, intellectual disability, hypotonia, hyperkinetic
305 movements and sleep disturbances. A consistent feature of Cav2.3 variants associated with
306 epilepsy is GoF of the channel, by left-shifting the activation voltage, altering maximal current
307 and/or by slowing inactivation [41]. Our data shows that deletion of CDKL5 results in loss of
308 Cav2.3 S15 phosphorylation, leading to GoF due to slowed inactivation and amplified gating
309 modulation, similar to the effects observed in Cav2.3 variants. Our results establish Cav2.3
310 overactivity as a common feature of CACNA1E (DEE69) and CDKL5 (DEE2) epileptic
311 encephalopathies, potentially explaining overlapping clinical features of these diseases.

312 Cytoplasmic N-terminal S15 phosphorylation of Cav2.3 has been previously detected in global
313 phosphoproteomics screens from brain (phosphosite.org), but the responsible kinase and the
314 role of this phosphorylation were unknown. N-terminal deletions in Cav2.3 [57] or the related
315 Cav2.2 [77, 78], result in channels with normal gating and conduction properties. Inactivation

316 kinetics were not measured in these studies, yet interestingly Cav2.2 N-terminal deletion
317 mutants seemed to have slower decaying currents, indicating that this region participates in
318 the regulation of inactivation [77]. Analogously, loss of N-terminal Ser14/15 phosphorylation
319 slows Cav2.3 inactivation in HEK293 cells and neurons, underscoring a previously overlooked
320 regulatory role of the Cav2.3 N-terminus. This domain may interact with Cavβ, as previously
321 suggested for Cav2.2 [78].

322 We also find that cholinergic stimulation amplifies Cav2.3 GoF in absence of CDKL5
323 phosphorylation, by prominently shifting activation $V_{1/2}$ and increasing currents at maximal
324 activation voltages, thus revealing a second molecular mechanism by which loss of pS14/15
325 enhances Cav2.3 function. It is known that muscarinic enhancement of Cav2.3 depends on
326 Gαq signalling and PKC phosphorylation at multiple sites, including the intracellular loop I-II
327 [59], the most prominent site of α1-β interaction [51]. We show that loss of pS14 interferes with
328 PKC enhancement upon carbachol application, but the mechanisms of this interplay are yet
329 to be established.

330 Our recordings from hippocampal neurons in Cav2.3 S15A mice demonstrate that S15
331 regulates Cav2.3 function in neurons. We show that pS15 is critical for R-type current
332 inactivation and regulation of firing by cholinergic stimulation. Isolating Cav2.3 currents is
333 challenging due to space clamp limitations and the need for inhibitors of other voltage-gated
334 channels. These drugs may have promiscuous effects on Cav2.3 [79] or incompletely block other
335 Ca^{2+} currents (Tai et al., 2006). We observed enhanced neuronal excitability and increased
336 pro-epileptiform cholinergic ADPs/DPPs [56, 61] in Cav2.3 phosphomutant mice, an effect that
337 was not linked to carbachol suppression of AHPs or other intrinsic excitability properties in
338 these cells. Instead, we suggest that the GoF of unphosphorylated Cav2.3 underlies the hyper-
339 excitability seen in response to muscarinic stimulation. Interestingly, CDKL5 KO mice have
340 altered cholinergic tone [80] and the muscarinic antagonist Solifenacin was shown to ameliorate
341 network defects in CDD patient-derived neurons [81], supporting an enhanced cholinergic
342 modulation in this human model.

343 We find striking behavioural similarities between our Cav2.3 phosphomutant mice and CDKL5
344 KOs. Specifically, S15A mice showed reduced encoding and retention of fear memory, a
345 robust phenotype identified by several groups in CDKL5 KO models [14, 71, 72]. In contrast, Cav2.3
346 KO mice display enhanced fear [35]. Home-cage behaviour and social interaction phenotypes
347 are also common between Cav2.3 phosphomutant and CDKL5 KO mice [46, 71]. The deficits
348 observed in voluntary wheel in Cav2.3 phosphomutants could be indicative of mild hypotonia
349 [82, 83]. Importantly, these phosphomutant mouse phenotypes mirror human clinical
350 manifestations of CDD, arguing that slowed inactivation and enhanced cholinergic modulation
351 of unphosphorylated Cav2.3 may contribute to these symptoms.

352 Cav2.3 KO mice exhibit reduced susceptibility to chemical absence seizures [84-86] and
353 hippocampal KA-induced seizures [49]. In agreement with Cav2.3's role in epilepsy, we find
354 increased seizure susceptibility in females in the low-dose KA injection paradigm in our Cav2.3
355 S15A mice. The difference between males and females, observed in both ECoG and
356 behavioural seizure analysis, may arise from increased basal function of Cav2.3 in the female
357 brain downstream of hormonal signals. Gender should be taken into consideration in future
358 mouse CDKL5 KO studies, where KA-induced seizure susceptibility changes have not been
359 observed [17, 46] and susceptibility to other chemoconvulsants were reported [72] but not widely
360 reproduced [17]. Disturbance-associated seizure-like events have been observed in aged
361 heterozygous females in two different CDD mouse models (PMID: 33197557), an occurrence
362 that may be linked to developmental changes in Cav2.3 regulation.

363 In rodents, it is possible to reverse adult phenotypes with reintroduction of CDKL5 genetically
364 [70] or using AAV viruses [87], indicating an open therapeutic window for treatment. Here, we
365 report a novel functional regulation of Cav2.3 by CDKL5 phosphorylation, which impinges of
366 neuronal excitability. Thus Cav2.3 GoF in absence of CDKL5 may be an important molecular
367 mechanism in CDD pathology. In addition to CACNA1E encephalopathy, increased Ca^{2+} influx
368 through Cav2.3 may contribute to epileptogenesis in Fragile X syndrome [88] and juvenile
369 myoclonic epilepsy [89]. Cav2.3 also increases susceptibility to drug-induced Parkinson's
370 disease [90, 91]. We propose that Cav2.3 inhibitors/ modulators could be beneficial for CDD
371 patients and potentially for a broader population of neurological patients in the future.

372

373

374

375

376

377

378

379

380

381

382

383

Acknowledgements

We thank Ultanir lab members for valuable discussion and thoughtful comments. We thank Helen Flynn for valuable assistance with mass spectrometry. We thank Crick GEMS team for creation of CACNA1E S15A mice. This work was supported by the Francis Crick Institute which receives its core funding from Cancer Research UK (CC2037), the UK Medical Research Council (CC2037), and the Wellcome Trust (CC2037); Loulou Foundation Project Grant (11015); Crick-MSD Framework collaboration grant (11202). For the purpose of Open Access, the author has applied a CC BY public copyright licence to any Author Accepted Manuscript version arising from this submission.

Author contributions

MSC, LLB, GL and SKU designed the experiments. MSC performed and analysed electrophysiology and biochemistry experiments. LLB performed mass spectrometry. YQ and GL conducted/ analysed EEG and kainic acid-induced seizure experiments. ATL and MSC performed behaviour experiments/ analysis. LS, SM, SC provided technical assistance in molecular biology and electrophysiology. MSC and SKU wrote the initial version of the manuscript. JR contributed to the original draft and review/editing along with all authors.

Declaration of interests

The authors declare no competing interest.

Inclusion and diversity

We ensured the sex balance in our mouse cohorts. Authors in this paper have balanced gender representation. This manuscript includes authors with diverse race, ethnicity, and sexual orientation.

415 ***References***

416

417 1. Kalscheuer, V.M.*, et al.* Disruption of the serine/threonine kinase 9 gene causes severe X-
418 linked infantile spasms and mental retardation. *American journal of human genetics* **72**, 1401-1411
419 (2003).
420 2. Olson, H.E.*, et al.* Cyclin-Dependent Kinase-Like 5 Deficiency Disorder: Clinical Review. *Pediatr*
421 *Neurol* **97**, 18-25 (2019).
422 3. Van Bergen, N.J.*, et al.* CDKL5 deficiency disorder: molecular insights and mechanisms of
423 pathogenicity to fast-track therapeutic development. *Biochemical Society transactions* **50**, 1207-1224
424 (2022).
425 4. Leonard, H.*, et al.* CDKL5 deficiency disorder: clinical features, diagnosis, and management.
426 *Lancet Neurol* **21**, 563-576 (2022).
427 5. Munoz, I.M.*, et al.* Phosphoproteomic screening identifies physiological substrates of the
428 CDKL5 kinase. *The EMBO journal* **37** (2018).
429 6. Hector, R.D.*, et al.* CDKL5 variants: Improving our understanding of a rare neurologic disorder.
430 *Neurol Genet* **3**, e200 (2017).
431 7. Krishnaraj, R., Ho, G. & Christodoulou, J. RettBASE: Rett syndrome database update. *Human*
432 *mutation* **38**, 922-931 (2017).
433 8. Bahi-Buisson, N.*, et al.* Recurrent mutations in the CDKL5 gene: genotype-phenotype
434 relationships. *American journal of medical genetics. Part A* **158A**, 1612-1619 (2012).
435 9. Symonds, J.D.*, et al.* Incidence and phenotypes of childhood-onset genetic epilepsies: a
436 prospective population-based national cohort. *Brain : a journal of neurology* **142**, 2303-2318 (2019).
437 10. Lindy, A.S.*, et al.* Diagnostic outcomes for genetic testing of 70 genes in 8565 patients with
438 epilepsy and neurodevelopmental disorders. *Epilepsia* **59**, 1062-1071 (2018).
439 11. Kothur, K.*, et al.* Diagnostic yield of targeted massively parallel sequencing in children with
440 epileptic encephalopathy. *Seizure* **59**, 132-140 (2018).
441 12. Bahi-Buisson, N. & Bienvenu, T. CDKL5-Related Disorders: From Clinical Description to
442 Molecular Genetics. *Mol Syndromol* **2**, 137-152 (2012).
443 13. Siri, B.*, et al.* CDKL5 deficiency disorder in males: Five new variants and review of the literature.
444 *Eur J Paediatr Neurol* **33**, 9-20 (2021).
445 14. Wang, I.T.*, et al.* Loss of CDKL5 disrupts kinome profile and event-related potentials leading
446 to autistic-like phenotypes in mice. *Proceedings of the National Academy of Sciences of the United*
447 *States of America* **109**, 21516-21521 (2012).
448 15. Hector, R.D.*, et al.* Characterisation of CDKL5 Transcript Isoforms in Human and Mouse. *PloS*
449 *one* **11**, e0157758 (2016).
450 16. Hector, R.D.*, et al.* Characterisation of Cdkl5 transcript isoforms in rat. *Gene* **603**, 21-26 (2017).
451 17. Okuda, K.*, et al.* CDKL5 controls postsynaptic localization of GluN2B-containing NMDA
452 receptors in the hippocampus and regulates seizure susceptibility. *Neurobiology of disease* **106**, 158-
453 170 (2017).
454 18. Rusconi, L.*, et al.* CDKL5 expression is modulated during neuronal development and its
455 subcellular distribution is tightly regulated by the C-terminal tail. *The Journal of biological chemistry*
456 **283**, 30101-30111 (2008).
457 19. Baltussen, L.L.*, et al.* Chemical genetic identification of CDKL5 substrates reveals its role in
458 neuronal microtubule dynamics. *The EMBO journal* **37** (2018).
459 20. Khanam, T.*, et al.* CDKL5 kinase controls transcription-coupled responses to DNA damage. *The*
460 *EMBO journal* **40**, e108271 (2021).
461 21. Kim, J.Y.*, et al.* A kinome-wide screen identifies a CDKL5-SOX9 regulatory axis in epithelial cell
462 death and kidney injury. *Nat Commun* **11**, 1924 (2020).
463 22. Zhou, A., Han, S. & Zhou, Z.J. Molecular and genetic insights into an infantile epileptic
464 encephalopathy - CDKL5 disorder. *Front Biol (Beijing)* **12**, 1-6 (2017).

465 23. Katayama, S., Sueyoshi, N., Inazu, T. & Kameshita, I. Cyclin-Dependent Kinase-Like 5 (CDKL5):
466 Possible Cellular Signalling Targets and Involvement in CDKL5 Deficiency Disorder. *Neural plasticity*
467 **2020**, 6970190 (2020).
468 24. Gurgone, A*., et al.* mGluR5 PAMs rescue cortical and behavioural defects in a mouse model of
469 CDKL5 deficiency disorder. *Neuropsychopharmacology* (2022).
470 25. La Montanara, P*., et al.* Cyclin-dependent-like kinase 5 is required for pain signaling in human
471 sensory neurons and mouse models. *Sci Transl Med* **12** (2020).
472 26. Di Nardo, A*., et al.* Phenotypic characterization of Cdkl5-knockdown neurons establishes
473 elongated cilia as a functional assay for CDKL5 Deficiency Disorder. *Neuroscience research* **176**, 73-78
474 (2022).
475 27. Kontaxi, C., Davenport, E.C., Kind, P.C. & Cousin, M.A. Epilepsy-related CDKL5 deficiency slows
476 synaptic vesicle endocytosis in central nerve terminals. *bioRxiv*, 2022.2003.2015.484308 (2022).
477 28. Halpain, S. & Dehmelt, L. The MAP1 family of microtubule-associated proteins. *Genome*
478 *biology* **7**, 224 (2006).
479 29. Huang, J. & Zamponi, G.W. Regulation of voltage gated calcium channels by GPCRs and post-
480 translational modification. *Curr Opin Pharmacol* **32**, 1-8 (2017).
481 30. Zamponi, G.W. Targeting voltage-gated calcium channels in neurological and psychiatric
482 diseases. *Nature reviews. Drug discovery* **15**, 19-34 (2016).
483 31. Dietrich, D*., et al.* Functional specialization of presynaptic Cav2.3 Ca2+ channels. *Neuron* **39**,
484 483-496 (2003).
485 32. Parajuli, L.K*., et al.* Quantitative regional and ultrastructural localization of the Ca(v)2.3
486 subunit of R-type calcium channel in mouse brain. *J Neurosci* **32**, 13555-13567 (2012).
487 33. Sochivko, D*., et al.* The Ca(V)2.3 Ca(2+) channel subunit contributes to R-type Ca(2+) currents
488 in murine hippocampal and neocortical neurones. *The Journal of physiology* **542**, 699-710 (2002).
489 34. Zhang, J.F*., et al.* Distinctive pharmacology and kinetics of cloned neuronal Ca2+ channels and
490 their possible counterparts in mammalian CNS neurons. *Neuropharmacology* **32**, 1075-1088 (1993).
491 35. Lee, S.C*., et al.* Molecular basis of R-type calcium channels in central amygdala neurons of the
492 mouse. *Proceedings of the National Academy of Sciences of the United States of America* **99**, 3276-
493 3281 (2002).
494 36. Schneider, T*., et al.* Molecular analysis and functional expression of the human type E neuronal
495 Ca2+ channel alpha 1 subunit. *Recept Channels* **2**, 255-270 (1994).
496 37. Soong, T.W*., et al.* Structure and functional expression of a member of the low voltage-
497 activated calcium channel family. *Science* **260**, 1133-1136 (1993).
498 38. Neumaier, F., Alpdogan, S., Hescheler, J. & Schneider, T. Protein phosphorylation maintains
499 the normal function of cloned human Cav2.3 channels. *J Gen Physiol* **150**, 491-510 (2018).
500 39. Schneider, T., Alpdogan, S., Hescheler, J. & Neumaier, F. In vitro and in vivo phosphorylation
501 of the Cav2.3 voltage-gated R-type calcium channel. *Channels (Austin)* **12**, 326-334 (2018).
502 40. Proft, J. & Weiss, N. G protein regulation of neuronal calcium channels: back to the future.
503 *Mol Pharmacol* **87**, 890-906 (2015).
504 41. Helbig, K.L*., et al.* De Novo Pathogenic Variants in CACNA1E Cause Developmental and
505 Epileptic Encephalopathy with Contractures, Macrocephaly, and Dyskinesias. *American journal of*
506 *human genetics* **103**, 666-678 (2018).
507 42. Heyne, H.O*., et al.* De novo variants in neurodevelopmental disorders with epilepsy. *Nature*
508 *genetics* **50**, 1048-1053 (2018).
509 43. Happ, H.C. & Carvill, G.L. A 2020 View on the Genetics of Developmental and Epileptic
510 Encephalopathies. *Epilepsy Curr* **20**, 90-96 (2020).
511 44. Steward, C.A*., et al.* Re-annotation of 191 developmental and epileptic encephalopathy-
512 associated genes unmasks de novo variants in SCN1A. *NPJ Genom Med* **4**, 31 (2019).
513 45. Mann, M. Functional and quantitative proteomics using SILAC. *Nature reviews. Molecular cell*
514 *biology* **7**, 952-958 (2006).
515 46. Amendola, E*., et al.* Mapping pathological phenotypes in a mouse model of CDKL5 disorder.
516 *PloS one* **9**, e91613 (2014).

517 47. Weiergraber, M.*, et al.* Altered seizure susceptibility in mice lacking the Ca(v)2.3 E-type Ca2+
518 channel. *Epilepsia* **47**, 839-850 (2006).
519 48. Weiergraber, M., Kamp, M.A., Radhakrishnan, K., Hescheler, J. & Schneider, T. The Ca(v)2.3
520 voltage-gated calcium channel in epileptogenesis--shedding new light on an enigmatic channel.
521 *Neurosci Biobehav Rev* **30**, 1122-1144 (2006).
522 49. Weiergraber, M., Henry, M., Radhakrishnan, K., Hescheler, J. & Schneider, T. Hippocampal
523 seizure resistance and reduced neuronal excitotoxicity in mice lacking the Cav2.3 E/R-type voltage-
524 gated calcium channel. *Journal of neurophysiology* **97**, 3660-3669 (2007).
525 50. Jones, L.P., Wei, S.K. & Yue, D.T. Mechanism of auxiliary subunit modulation of neuronal
526 alpha1E calcium channels. *J Gen Physiol* **112**, 125-143 (1998).
527 51. Buraei, Z. & Yang, J. The ss subunit of voltage-gated Ca2+ channels. *Physiol Rev* **90**, 1461-1506
528 (2010).
529 52. Muller, C.S.*, et al.* Quantitative proteomics of the Cav2 channel nano-environments in the
530 mammalian brain. *Proceedings of the National Academy of Sciences of the United States of America*
531 **107**, 14950-14957 (2010).
532 53. Tai, C., Kuzmiski, J.B. & MacVicar, B.A. Muscarinic enhancement of R-type calcium currents in
533 hippocampal CA1 pyramidal neurons. *J Neurosci* **26**, 6249-6258 (2006).
534 54. Bannister, R.A., Melliti, K. & Adams, B.A. Differential modulation of CaV2.3 Ca2+ channels by
535 Galphaq/11-coupled muscarinic receptors. *Mol Pharmacol* **65**, 381-388 (2004).
536 55. Meza, U., Bannister, R., Melliti, K. & Adams, B. Biphasic, opposing modulation of cloned
537 neuronal alpha1E Ca channels by distinct signaling pathways coupled to M2 muscarinic acetylcholine
538 receptors. *J Neurosci* **19**, 6806-6817 (1999).
539 56. Fraser, D.D. & MacVicar, B.A. Cholinergic-dependent plateau potential in hippocampal CA1
540 pyramidal neurons. *J Neurosci* **16**, 4113-4128 (1996).
541 57. Page, K.M., Canti, C., Stephens, G.J., Berrow, N.S. & Dolphin, A.C. Identification of the amino
542 terminus of neuronal Ca2+ channel alpha1 subunits alpha1B and alpha1E as an essential determinant
543 of G-protein modulation. *J Neurosci* **18**, 4815-4824 (1998).
544 58. Canti, C., Page, K.M., Stephens, G.J. & Dolphin, A.C. Identification of residues in the N terminus
545 of alpha1B critical for inhibition of the voltage-dependent calcium channel by Gbeta gamma. *J*
546 *Neurosci* **19**, 6855-6864 (1999).
547 59. Fang, H.*, et al.* Role of alpha1 2.3 subunit I-II linker sites in the enhancement of Ca(v) 2.3
548 current by phorbol 12-myristate 13-acetate and acetyl-beta-methylcholine. *The Journal of biological*
549 *chemistry* **280**, 23559-23565 (2005).
550 60. Buchanan, K.A., Petrovic, M.M., Chamberlain, S.E., Marrion, N.V. & Mellor, J.R. Facilitation of
551 long-term potentiation by muscarinic M(1) receptors is mediated by inhibition of SK channels. *Neuron*
552 **68**, 948-963 (2010).
553 61. Park, J.Y. & Spruston, N. Synergistic actions of metabotropic acetylcholine and glutamate
554 receptors on the excitability of hippocampal CA1 pyramidal neurons. *J Neurosci* **32**, 6081-6091 (2012).
555 62. Kawasaki, H., Palmieri, C. & Avoli, M. Muscarinic receptor activation induces depolarizing
556 plateau potentials in bursting neurons of the rat subiculum. *Journal of neurophysiology* **82**, 2590-2601
557 (1999).
558 63. Williams, S.R. & Fletcher, L.N. A Dendritic Substrate for the Cholinergic Control of Neocortical
559 Output Neurons. *Neuron* **101**, 486-499 e484 (2019).
560 64. Park, J.Y.*, et al.* A post-burst after depolarization is mediated by group i metabotropic
561 glutamate receptor-dependent upregulation of Ca(v)2.3 R-type calcium channels in CA1 pyramidal
562 neurons. *PLoS biology* **8**, e1000534 (2010).
563 65. Kuzmiski, J.B., Barr, W., Zamponi, G.W. & MacVicar, B.A. Topiramate inhibits the initiation of
564 plateau potentials in CA1 neurons by depressing R-type calcium channels. *Epilepsia* **46**, 481-489
565 (2005).
566 66. Brown, D.A. & Passmore, G.M. Neural KCNQ (Kv7) channels. *Br J Pharmacol* **156**, 1185-1195
567 (2009).
568 67. Stocker, M., Hirzel, K., D'Hoedt, D. & Pedarzani, P. Matching molecules to function: neuronal
569 Ca2+-activated K+ channels and afterhyperpolarizations. *Toxicon* **43**, 933-949 (2004).

68. Bloodgood, B.L. & Sabatini, B.L. Nonlinear regulation of unitary synaptic signals by CaV(2.3) voltage-sensitive calcium channels located in dendritic spines. *Neuron* **53**, 249-260 (2007).
69. Murphy, J.G.*, et al.* R-type voltage-gated Ca(2+) channels mediate A-type K(+) current regulation of synaptic input in hippocampal dendrites. *Cell Rep* **38**, 110264 (2022).
70. Terzic, B.*, et al.* Temporal manipulation of Cdkl5 reveals essential postdevelopmental functions and reversible CDKL5 deficiency disorder-related deficits. *J Clin Invest* **131** (2021).
71. Okuda, K.*, et al.* Comprehensive behavioral analysis of the Cdkl5 knockout mice revealed significant enhancement in anxiety- and fear-related behaviors and impairment in both acquisition and long-term retention of spatial reference memory. *PloS one* **13**, e0196587 (2018).
72. Yennawar, M., White, R.S. & Jensen, F.E. AMPA Receptor Dysregulation and Therapeutic Interventions in a Mouse Model of CDKL5 Deficiency Disorder. *J Neurosci* **39**, 4814-4828 (2019).
73. Terzic, B.*, et al.* X-linked cellular mosaicism underlies age-dependent occurrence of seizure-like events in mouse models of CDKL5 deficiency disorder. *Neurobiology of disease* **148**, 105176 (2021).
74. Wang, H.T.*, et al.* CDKL5 deficiency in forebrain glutamatergic neurons results in recurrent spontaneous seizures. *Epilepsia* **62**, 517-528 (2021).
75. Colasante, G.*, et al.* In vivo CRISPRa decreases seizures and rescues cognitive deficits in a rodent model of epilepsy. *Brain : a journal of neurology* **143**, 891-905 (2020).
76. Tse, K., Puttachary, S., Beamer, E., Sills, G.J. & Thippeswamy, T. Advantages of repeated low dose against single high dose of kainate in C57BL/6J mouse model of status epilepticus: behavioral and electroencephalographic studies. *PloS one* **9**, e96622 (2014).
77. Page, K.M.*, et al.* N terminus is key to the dominant negative suppression of Ca(V)2 calcium channels: implications for episodic ataxia type 2. *The Journal of biological chemistry* **285**, 835-844 (2010).
78. Stephens, G.J., Page, K.M., Bogdanov, Y. & Dolphin, A.C. The alpha1B Ca2+ channel amino terminus contributes determinants for beta subunit-mediated voltage-dependent inactivation properties. *The Journal of physiology* **525 Pt 2**, 377-390 (2000).
79. Williams, M.E.*, et al.* Structure and functional characterization of neuronal alpha 1E calcium channel subtypes. *The Journal of biological chemistry* **269**, 22347-22357 (1994).
80. Artoni, P.*, et al.* Deep learning of spontaneous arousal fluctuations detects early cholinergic defects across neurodevelopmental mouse models and patients. *Proceedings of the National Academy of Sciences of the United States of America* **117**, 23298-23303 (2020).
81. Negraes, P.D.*, et al.* Altered network and rescue of human neurons derived from individuals with early-onset genetic epilepsy. *Molecular psychiatry* **26**, 7047-7068 (2021).
82. Kamaludin, A.A.*, et al.* Muscle dysfunction caused by loss of Magel2 in a mouse model of Prader-Willi and Schaaf-Yang syndromes. *Human molecular genetics* **25**, 3798-3809 (2016).
83. Ruiz, A.*, et al.* Improvement of muscle strength in a mouse model for congenital myopathy treated with HDAC and DNA methyltransferase inhibitors. *eLife* **11** (2022).
84. Weiergraber, M.*, et al.* Altered thalamocortical rhythmicity in Ca(v)2.3-deficient mice. *Molecular and cellular neurosciences* **39**, 605-618 (2008).
85. Zaman, T.*, et al.* Cav2.3 channels are critical for oscillatory burst discharges in the reticular thalamus and absence epilepsy. *Neuron* **70**, 95-108 (2011).
86. Wormuth, C.*, et al.* Review: Cav2.3 R-type Voltage-Gated Ca(2+) Channels - Functional Implications in Convulsive and Non-convulsive Seizure Activity. *Open Neurol J* **10**, 99-126 (2016).
87. Gao, Y.*, et al.* Gene replacement ameliorates deficits in mouse and human models of cyclin-dependent kinase-like 5 disorder. *Brain : a journal of neurology* **143**, 811-832 (2020).
88. Gray, E.E.*, et al.* Disruption of GpI mGluR-Dependent Cav2.3 Translation in a Mouse Model of Fragile X Syndrome. *J Neurosci* **39**, 7453-7464 (2019).
89. Suzuki, T.*, et al.* Mutations in EFHC1 cause juvenile myoclonic epilepsy. *Nature genetics* **36**, 842-849 (2004).
90. Benkert, J.*, et al.* Cav2.3 channels contribute to dopaminergic neuron loss in a model of Parkinson's disease. *Nat Commun* **10**, 5094 (2019).

91. Siller, A.*, et al.* beta2-subunit alternative splicing stabilizes Cav2.3 Ca(2+) channel activity during continuous midbrain dopamine neuron-like activity. *eLife* **11** (2022).
92. Shakeri, B., Bourdin, B., Demers-Giroux, P.O., Sauve, R. & Parent, L. A quartet of leucine residues in the guanylate kinase domain of CaVbeta determines the plasma membrane density of the CaV2.3 channel. *The Journal of biological chemistry* **287**, 32835-32847 (2012).
93. Iannello, F. Non-intrusive high throughput automated data collection from the home cage. *Heliyon* **5**, e01454 (2019).

Figure 1

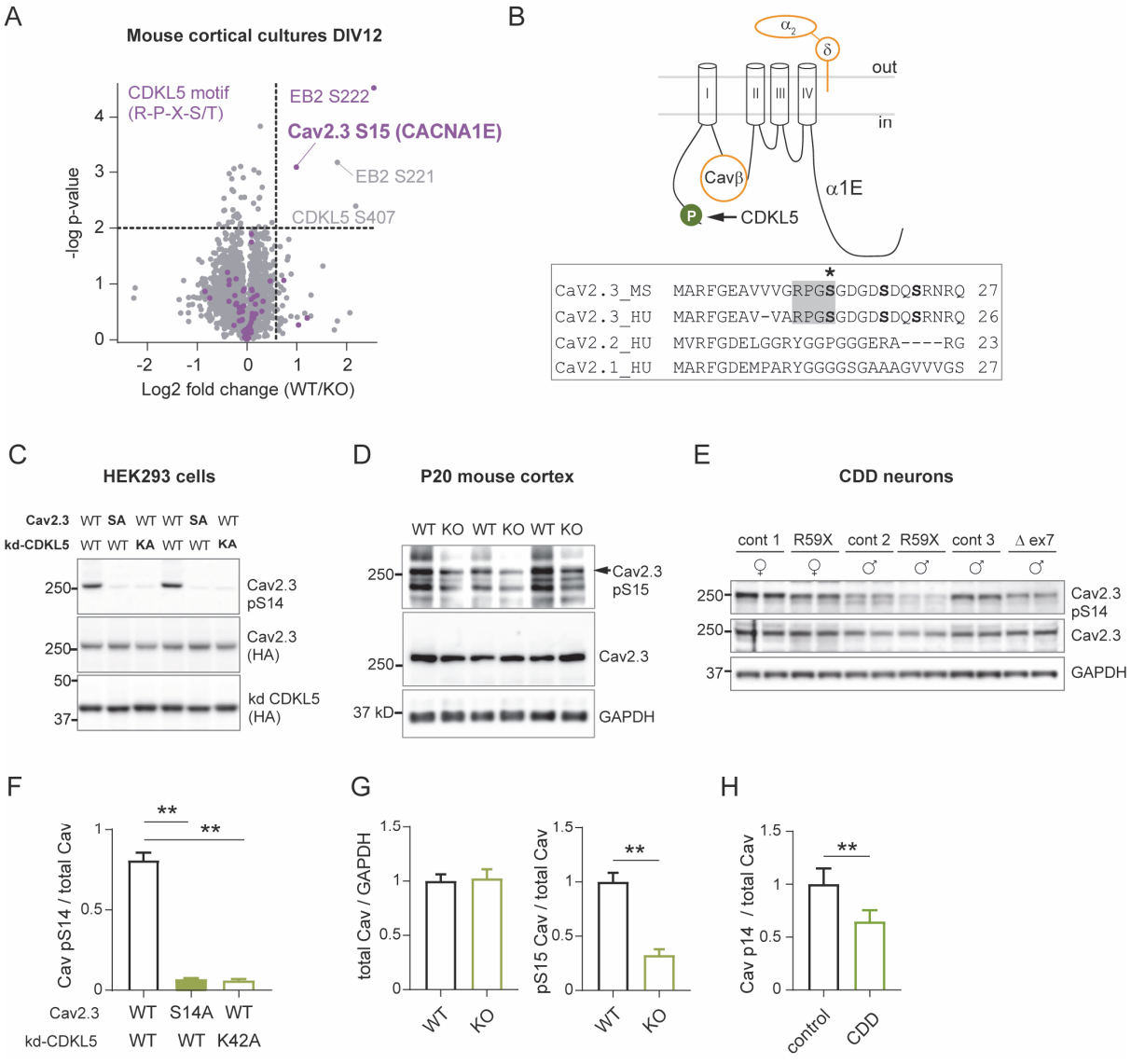

Figure 1. Identification and validation of Cav2.3 as substrate of CDKL5 kinase. A) Volcano plot of differential phosphoprotein levels between WT and CDKL5 KO primary neurons, obtained using SILAC based quantitative proteomics (5 embryos/genotype). Each point represents one peptide; those with CDKL5 consensus motif RPXS/T are highlighted in magenta. The x axis shows log2 transformed fold change in phosphopeptide levels between genotypes and the y axis shows significance as -log10 transformed p value. Significant was established as indicated by the dotted lines ($p<0.01$, fold change 1.5, one sample t test). B) Top: Schematic depiction of Cav2.3 formed of α1E channel pore subunit and associated proteins Cavβ and α2δ. CDKL5 phosphorylation site at α1E S15/14 is highlighted in green. Bottom: Alignment of proximal N-terminus of mouse and human Cav2.3 and related human Cav2.1 and 2.2 channel proteins. *S is the site of CDKL5 phosphorylation. C) Western blot of

658 HEK293 cells stably expressing human β3/α2δ1 subunits and transiently co-transfected with
659 human HA-α1E (Cav2.3: WT or S14A mutant) and HA-CDKL5 kinase domain (kd CDKL5: WT
660 or K42A mutant). S14 phosphorylation (pS14 Cav2.3) was detected with a custom made
661 phosphoantibody. D) Western blot of P20 cortices from WT and CDKL5 KO mice. E) Western
662 blot of iPSC-derived forebrain neurons from three CDD patients and related controls (parents)
663 at 6 weeks of differentiation. Gender and *CDKL5* mutation are specified [81]. F) Quantification
664 for immunoblot in C (**p<0.01 Kruskal-Wallis ANOVA & Dunn's test, n=11, 4 blots, 2
665 transfections). G) Quantification for immunoblot in D (**p<0.01 unpaired t test, n=9, 3 blots, 6
666 mice/genotype). H) Quantification for WB in E (**p<0.01 paired t test, n=6, 2 blots, 2 technical
667 replicates). For antibodies used see Materials and methods.

668

Figure 2

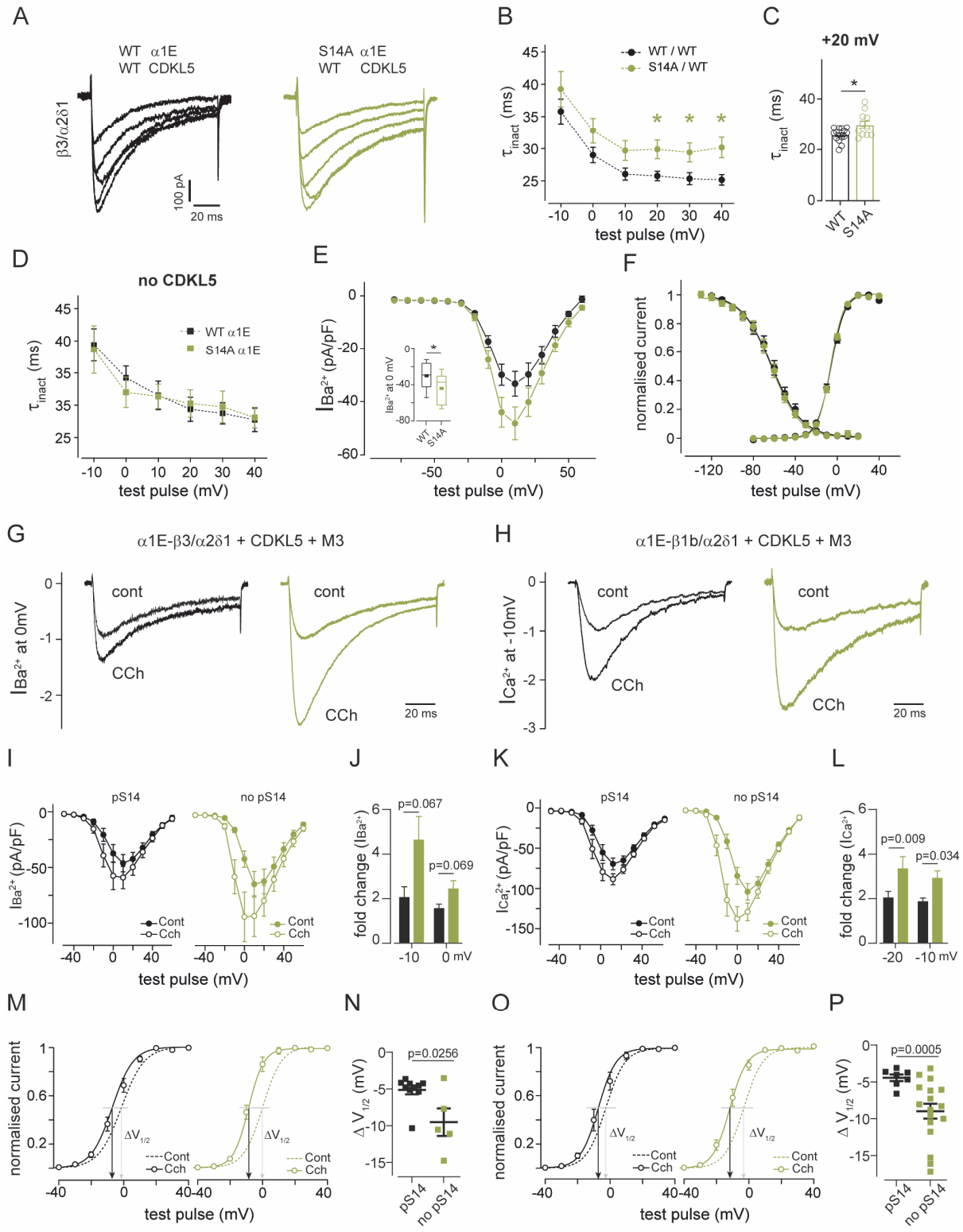

Figure 2. Functional characterization of phospho-Ser14 Cav2.3 in HEK 293 cells. A) Representative depolarization-evoked current responses in HEK293 cells stably expressing human β3/α2δ1 subunits and co-transfected with human Cav2.3 (WT α1E or S14A α1E) and

674 FLAG-CDKL5 full length (WT CDKL5). Construct combinations are presented in different
675 colours. Traces show steps from -10 to +30mV from a holding potential of -80mV and Ba^{2+} as
676 charge carrier B) Open channel inactivation tau (τ_{inact}) for Cav2.3 with (WT/WT, n=13-15) and
677 without (S14A/WT, n=11-13) CDKL5 phosphorylation (*p<0.05, TW ANOVA, Fisher's LSD).
678 Data were acquired using 100ms voltage steps from -80mV in +10mV increments every 10s.
679 C) Individual data points for τ_{inact} at +20mV (*p<0.05, unpaired t test). D) WT or phophomutant
680 S14A Cav2.3 inactivation in the same cell line in absence of CDKL5 (n=7-9; p>0.05 TW
681 ANOVA). Ca^{2+} was charge carrier. E) Current voltage relationship for cells in B. Inset:
682 comparison of current density at 0mV (inset, *p<0.05, unpaired t test). F) Normalised Cav2.3
683 current conductance and voltage dependence of inactivation for the same transfection
684 conditions. Activation $V_{1/2,}$ n: WT/WT -6±1 mV, 15; S14A/WT -6±1 mV,12; Inactivation $V_{1/2}$, n:
685 WT/WT -61±3 mV,10; S14A/WT -62±2 mV,11 (p>0.05, unpaired t test). For inactivation
686 protocol see Methods. Solid lines are Boltzman fits to the average data points G) Normalised
687 Ba^{2+} currents in the β3/α2δ1-cell line or H) Ca^{2+} currents in the β1/α2δ1-cell line, co-transfected
688 with α1E (WT or S14A), WT CDKL5 and muscarinic type 3 receptor (M3), in presence and
689 absence of carbachol (CCh) 30 and 10 μM, respectively. HP= -100mV. I) IV curves and J)
690 CCh-induced change in current amplitude for experiment in G (pS14 n=8, no pS14 n=7, TW
691 ANOVA, Fisher's LSD). K) IV curves and L) CCh-induced change in current amplitude for
692 experiment in H (pS14 n=7, no pS14 n=16 , TW ANOVA, Fisher's LSD). M) Conductance plots
693 for experiment in G and N) corresponding change in activation ($V_{1/2}$: -5±0.6 *vs*. -10±1.9 mV,
694 Kolmogorov-Smirnov). O) Conductance plots for experiment in H and P) corresponding
695 change in activation ($V_{1/2}$: -4±0.5 *vs* -9±1 mV, Welch's t test). From I-P, 'pS14' refers to WT
696 α1E/WT CDKL5; 'no pS14' refers to S14A α1E /WT CDKL5 and α1E WT /K42R* CDKL5
697 conditions pulled together.

698

699

Figure 3

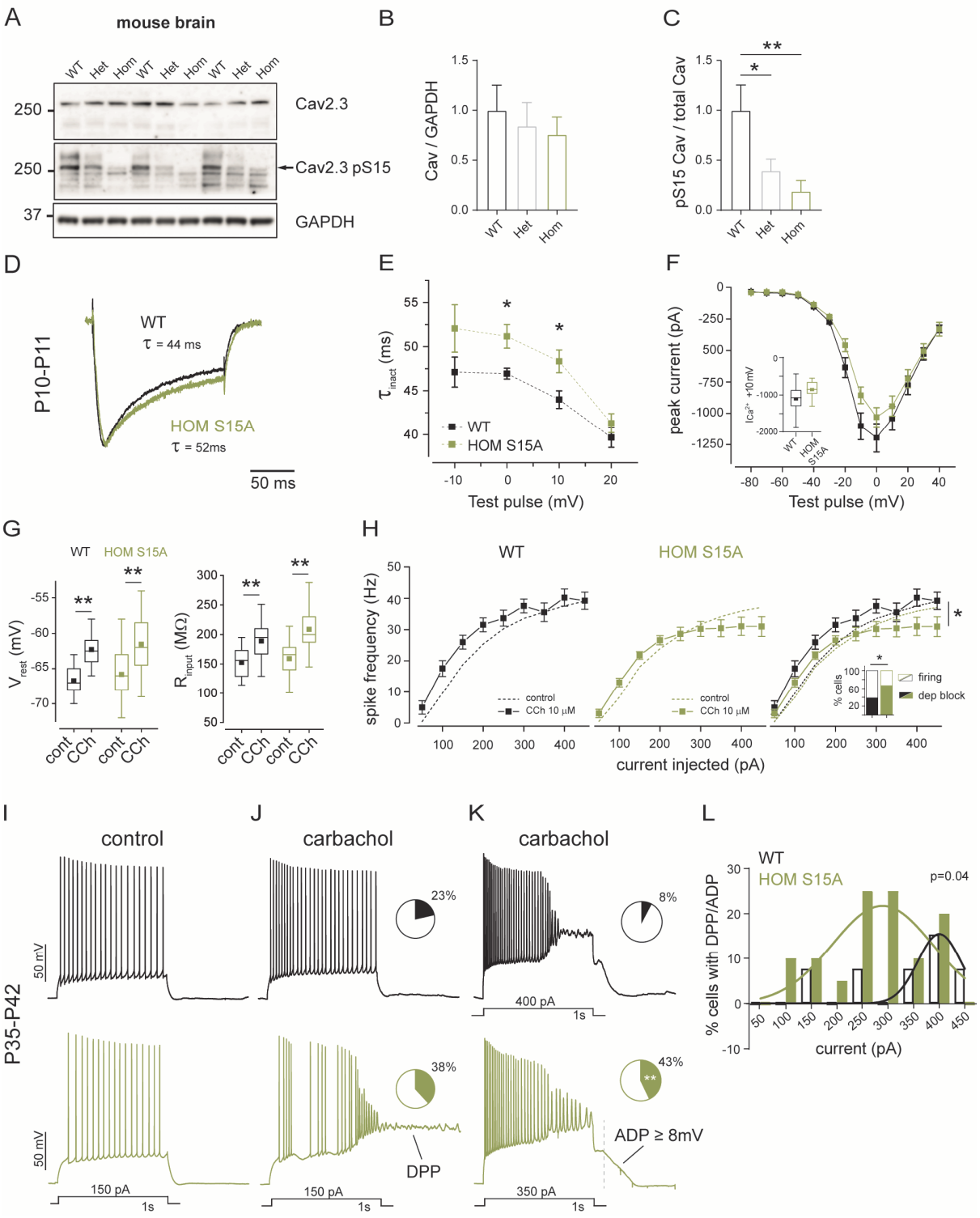

Figure 3. **Physiological properties and cholinergic neuromodulation of hippocampal CA1 neurons from WT and phosphomutant mice.** A) WB validation of CRISPR-generated Cav2.3 Ser15Ala mutant mice using a pS15 phosphoantibody in whole-brain lysates from 12-week-old WT, Heterozygous S15A and Homozygous S15A mice. B) Quantification of total

706 Cav2.3 ($p>0.05$ one way ANOVA) and C) relative phospho-S15 Cav2.3 (*$p<0.05$, **0.01 one-
707 way ANOVA, Fisher's LSD) expression (n=5, 2 blots, 3 mice/genotype). D) Normalised R-type
708 Ca^{2+} current in neurons from young mice of each genotype during a step from -60 to 0 mV in
709 presence of Na^{+}, K^{+}, Ca^{2+} and synaptic channel inhibitors. E) R-type current inactivation tau
710 (τ_{inact}) at maximal activation voltages (*$p<0.05$ TW RM ANOVA, Fisher's LSD) and F) average
711 IV curve for all P10-11cells recorded ($p>0.05$), (n=13 neurons, 4-5 mice/genotype). Data for -
712 10mV step is shown in the inset ($p=0.06$, unpaired t test). G) Membrane resting potential (V_{rest},
713 left) and input resistance (R_{input}, right) of adult neurons (WT n=13, HOM S15A n=17; 7
714 mice/genotype) in control conditions and after 10μM carbachol (CCh) application (**$p<0.01$,
715 paired t test). H) Input/output curves for the same neurons (WT n=9, HOM n=13, *$p<0.05$ TW
716 RM ANOVA) and percentage of cells with CCh-induced depolarization block (inset, WT n=13,
717 HOM n=21, *$p<0.05$, binomial test). I) Representative control action potential trains evoked in
718 WT (top) and HOM S15A (bottom) CA1 cells by 1s-long current injections. Membrane was
719 held at -65mV. J) Same cells as I upon application of CCh and representative depolarising
720 plateau potential (DPP), observed at some current injections in both genotypes; insets: fraction
721 of cells with at least one DPP in each genotype group (WT n=13, HOM n=21, $p>0.05$ binomial
722 test). K) Same cells as J at higher stimulation illustrating sustained depolarization and AP
723 block (top) or attenuation (bottom) towards the end of the stimulus and long-lasting large
724 amplitude afterdepolarizations (ADP). Like DPPs, these ADPs were present at some current
725 injections in a fraction of cells in both groups of mice (inset, WT n=13, HOM n=21, **$p<0.01$,
726 binomial test). L) Percentage of cells displaying sustained DPPs or ADPs upon stimulus
727 termination at each current injection step (non-linear fit comparison).

728

Figure 4

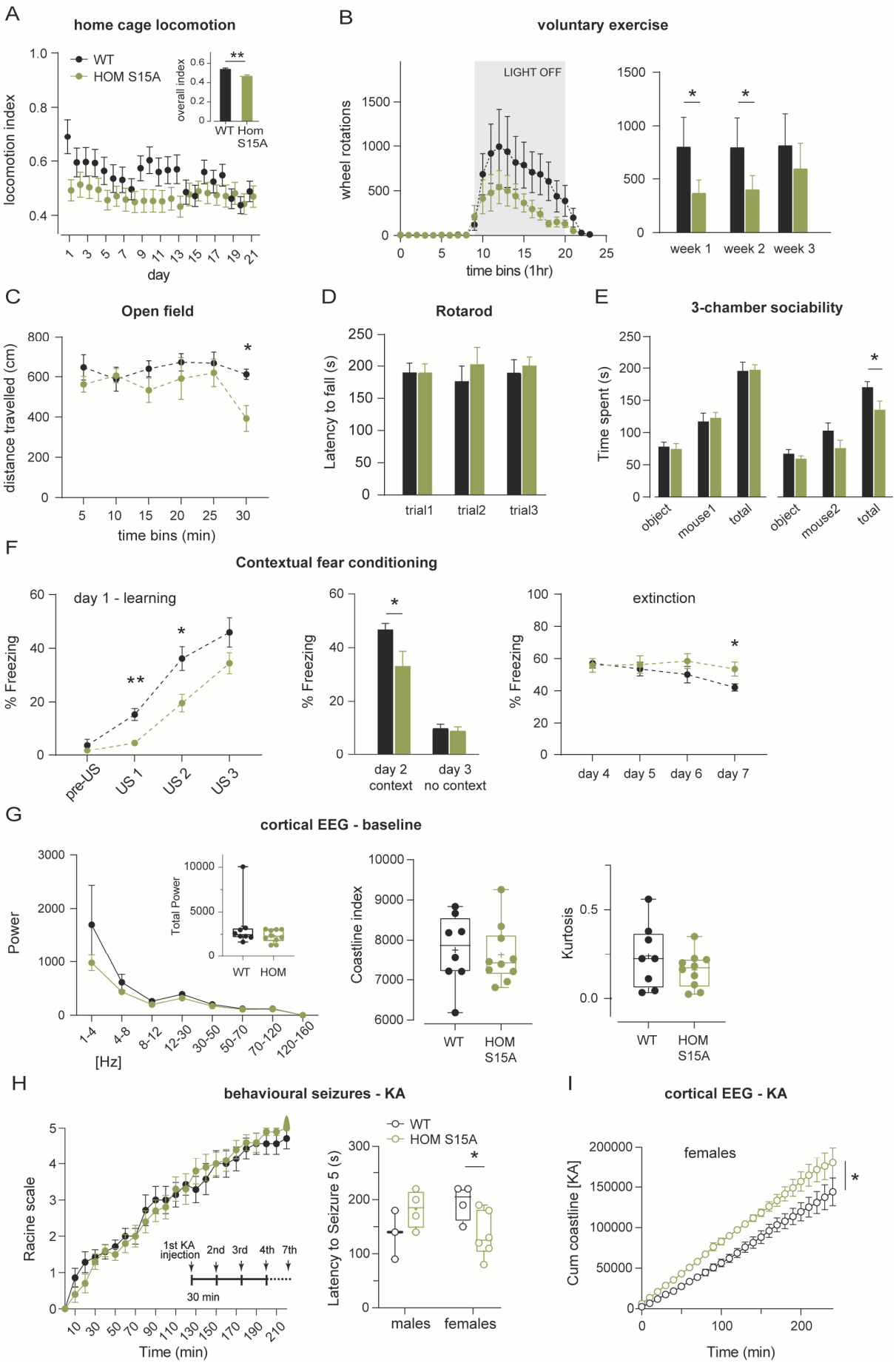
A
home cage locomotion
WT
HOM S15A
locomotion index
overall index
WT Hom S15A
day
B
voluntary exercise
LIGHT OFF
wheel rotations
time bins (1hr)
week 1
week 2
week 3
C
Open field
distance travelled (cm)
time bins (min)
D
Rotarod
Latency to fall (s)
trial1
trial2
trial3
E
3-chamber sociability
Time spent (s)
object
mouse1
total
object
mouse2
total
F
Contextual fear conditioning
day 1 - learning
% Freezing
pre-US
US 1
US 2
US 3
day 2 context
day 3 no context
extinction
day 4
day 5
day 6
day 7
G
cortical EEG - baseline
Power
Total Power
WT
HOM
[Hz]
1-4
4-8
8-12
12-30
30-50
50-70
70-120
120-160
Coastline index
Kurtosis
WT
HOM S15A
H
behavioural seizures - KA
Racine scale
1st KA injection
2nd
3rd
4th
7th
30 min
Time (min)
Latency to Seizure 5 (s)
males
females
I
cortical EEG - KA
females
Cum coastline [KA]
Time (min)

729

730 **Figure 4. *In vivo* phenotypic characterization of Cav2.3 S15A mice**. A) Average home
731 cage night-time locomotion of WT and HOM S15A mice (N=9) per day and overall locomotion
732 index (inset) in a three-week period (**p<0.01, Welch's t test). B) left: wheel rotations per hour
733 during voluntary exercise activity for the same mouse cohort as A, over a two-week period;
734 right: overall dark cycle average rotations in each group for three consecutive weeks (p<0.05
735 TW ANOVA, Fisher's LSD). C) Total distance travelled by WT (N=8) and HOMS15A (n=7)
736 mice in an open field arena (p<0.05 at 30 min TW ANOVA, Fisher's LSD). D) Accelerating
737 rotarod performance for the same cohort as C (p>0.05, TW ANOVA). Animal weights were
738 equal (WT=25±4 g, HOM=25±5 g, p>0.05, unpaired t test). E) Social, non-social and total
739 exploration times during a 10min three-chamber sociability test (p<0.05, unpaired t test). In
740 habituation trials, chamber occupancy was equal between groups. F) Freezing behaviour
741 during learning day 1 (left), associative memory test day 2+3 (middle) and memory extinction
742 test days 4-7 (right), in a fear-conditioning experiment with tactile and olfactory cues (*p<0.05
743 or **0.01, TW RM ANOVA, Fisher's LSD or unpaired t test). G) left: two-week baseline ECoG
744 spectral analysis and total power (inset) in WT (N=8) and HOMS15A (N=10) 9-12 week-old
745 mice; corresponding coastline index (middle) and kurtosis (right) (p>0.05, TW ANOVA and
746 unpaired t tests). No sex differences were observed. H) left: behavioural scoring of kainic acid
747 (KA)-induced seizures (WT N=7, HOMS15A N=10, p>0.05, TW ANOVA) using repetitive
748 5mg/kg i.p. injections (inset); right: latency to stage 5 tonic clonic seizures per gender (males,
749 p>0.05; females *p<0.05, unpaired t test). I) Corresponding cumulative ECoG coastline during
750 KA seizures in females (WT N=3, HOM S15A N=4, *p<0.05, TW ANOVA).

751

752

753

754

755

756

757

758

759

760

761

762

763 **Supplementary Figures**

764

Figure S1

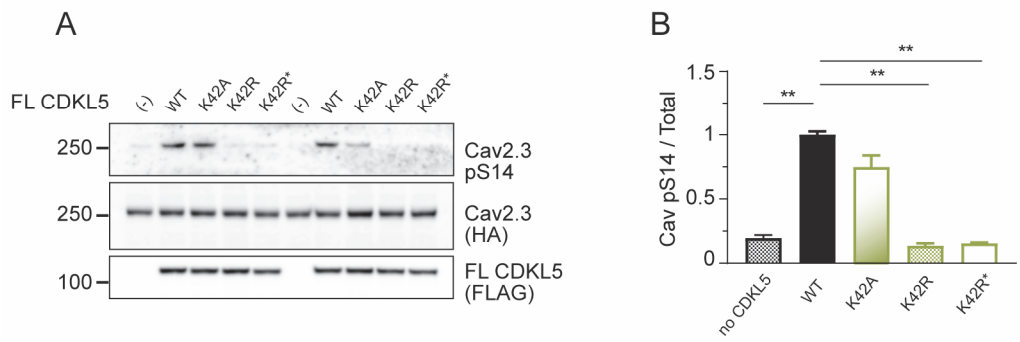

765

766

767 **FigureS1. Full-length CDKL5 phosphorylates Cav2.3.** A) Western blot of HEK293 cells
768 stably expressing human β3/α2δ1 subunits and transiently co-transfected with human WT HA-
769 α1E (Cav2.3) and FLAG-CDKL5 full length (FL CDKL5: WT, K42A, K42R, K42R*+DFG-AFG
770 kinase dead mutants). (-) transfection condition excludes CDKL5. The K42A mutation in FL-
771 CDKL5 retains some kinase activity on α1E, while K42R and K42R* mutants are fully inactive
772 and were thus selected for electrophysiology experiments. B) Quantification of relative
773 phospho-α1E (pS14 Cav2.3) levels for the experiment in A (**p<0.01, Brown-Forsythe &
774 Welch ANOVA, Dunnet's test; n=4-6, 3 blots, 2 transfections).

Figure S2

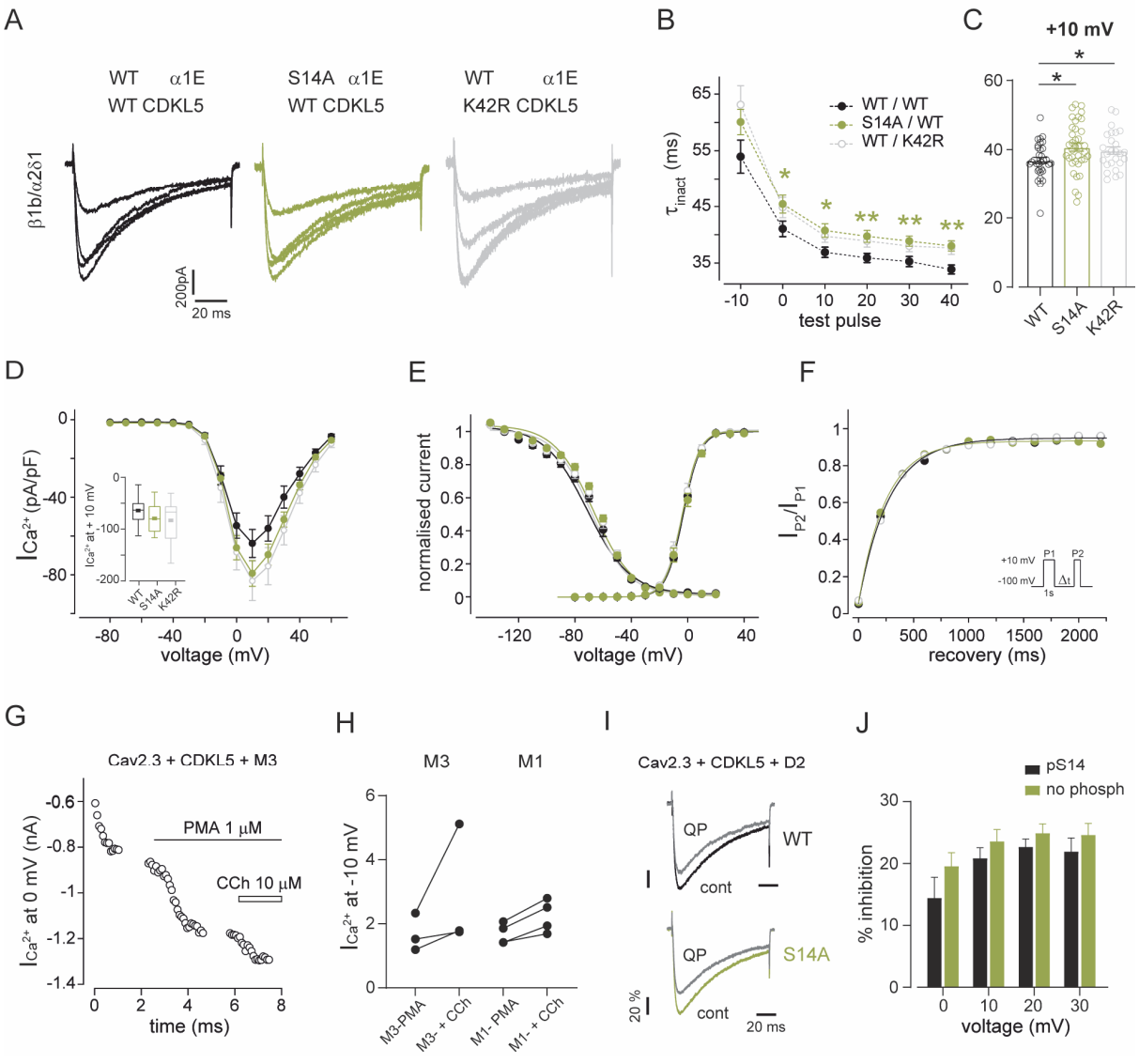

Figure S2. Functional characterization of phospho-Ser14 Cav2.3 in HEK 293 cells expressing β1 accessory subunit. A) Representative depolarization-evoked current responses in HEK293 cells stably expressing human β1/α2δ1 subunits and co-transfected with human Cav2.3 (WT α1E or S14A α1E mutant) and FLAG-CDKL5 full length (WT CDKL5 or K42R*+DFG-AFG kinase dead CDKL5 mutant). Construct combinations are presented in different colours. Traces show steps from -10 to +20mV from a holding potential of -100mV and Ca^{2+} as charge carrier. B) Open channel inactivation tau (τ_{inact}) for Cav2.3 with (WT/WT, n=28-32) and without (S14A/WT, n=34-37; WT/K45R, n=25-26) CDKL5 phosphorylation. WT/WT vs. S14A/WT: *p<0.05, **p<0.01 as indicated; WT/WT vs. WT/K42R*, p<0.01 at +40mV, p<0.05 at -10,10,20,30mV, TW ANOVA, Fisher's LSD. Some of the cells included in this plot co-expressed M3 receptors; this was *per se* not found to affect inactivation kinetics.

788 C) Individual data points for τ_{inact} at +10mV ($p<0.05$, unpaired t tests). D) Current-voltage
789 relationship for experiments in A (WT/WT, n=15; S14A/WT n=15-17; WT/K42R* n=12-15) and
790 current density at +10mV (inset, $p>0.05$, one way ANOVA). Data was acquired with 100ms
791 voltage steps from -100mV in +10mV increments every 10s. E) Normalised Cav2.3
792 conductance and voltage dependence of inactivation for the same three transfection
793 conditions. Activation $V_{1/2}$, n: WT/WT -3±1 mV, 14; S14A/WT -3±1 mV,17; WT/K42R* -2±1
794 mV, 14; Inactivation $V_{1/2}$, n: WT/WT -66±2 mV,14; S14A/WT -63±1 mV,14; WT/K42R* -65±2
795 mV,11 ($p>0.05$, one way ANOVA). For inactivation protocol see Methods. Solid lines are
796 Boltzman fits to the average data points. F) Inactivation recovery time using a double pulse
797 protocol with variable inter-pulse recovery time (inset). Recovery tau, n: WT/WT 265±21 ms,
798 4; S14A/WT 263±21 ms, 5; WT/K42R* 290±15 ms, 4, $p>0.05$ Kruskall-Wallis, Dunn's test). G)
799 Example time course of Cav2.3 current recording at 0mV in the β1/α2δ1-stable cell line co-
800 transfected with α1E WT, CDKL5 and muscarinic receptor type 3 (M3). PKC activation with
801 PMA did not occlude CCh enhancing effect. H) Relative change in current amplitude for same
802 experiment as G) with either M1 or M3 receptors. No muscarinic inhibition was observed. I)
803 Representative Cav2.3 current traces at +10mV in β1/α2δ1 stable cell line co-transfected with
804 α1E (WT or S14A), CDKL5 (WT) and dopamine receptor type 2 (D2). Quinpirole 100nM (QP)
805 application resulted in reliable and reversible inhibition of WT and S14A currents. J) Quantified
806 quinpirole inhibition of Cav2.3 with (n=7) or without pS14 (n=12-13) ($p>0.05$ TW ANOVA,
807 Fisher's LSD). Data for α1E S14A phosphomutant and K42R* CDKL5 conditions (no
808 phosphorylation) were pooled together.

Figure S3

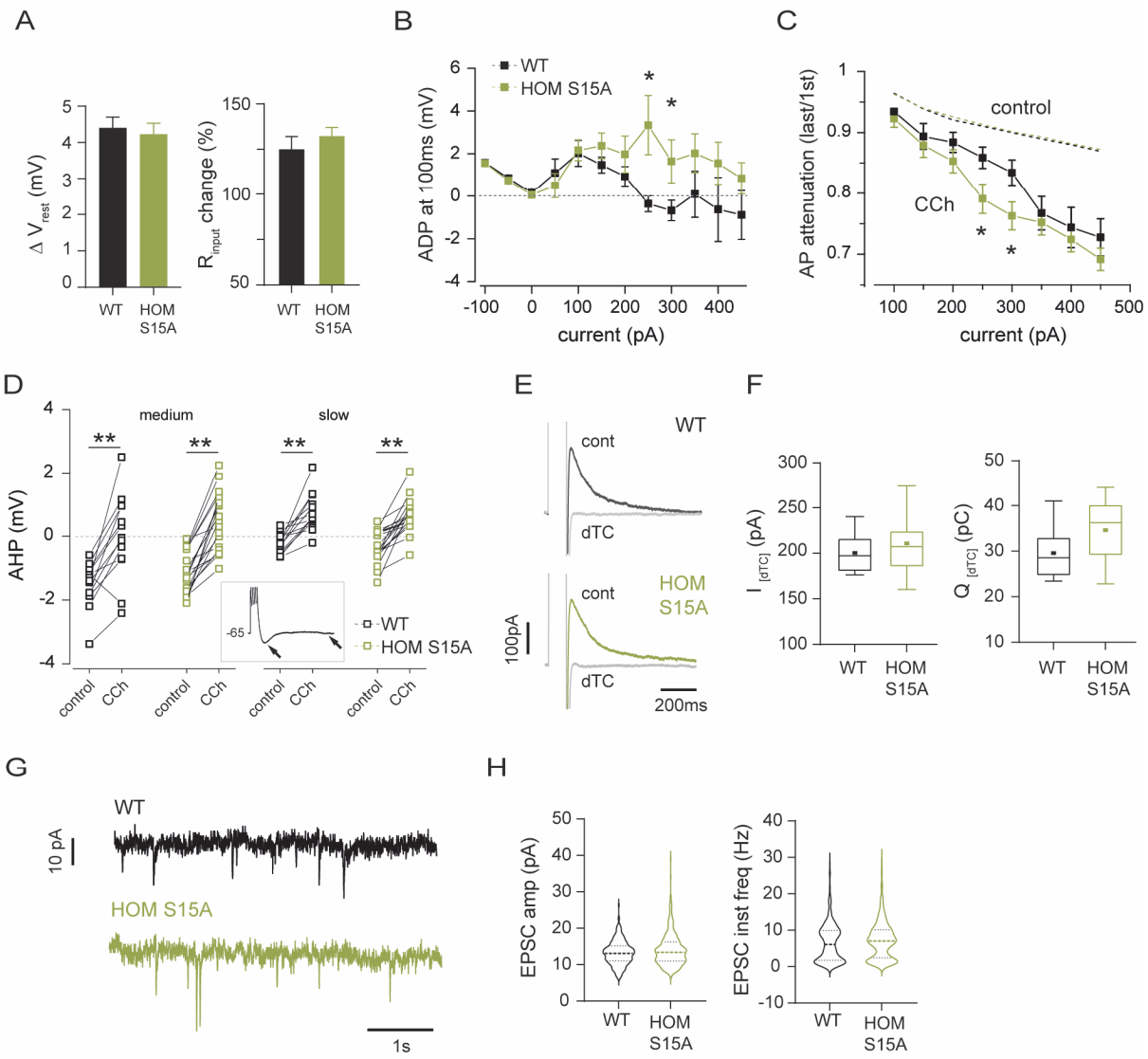

Figure S3. Additional CA1 neuron responses to carbachol and other intrinsic properties in adult WT and HOM S15A mice. A) Relative changes in membrane potential (V_{rest}) and resistance (R_{input}) upon 10 μM CCh application in WT (13) and HOM S15A (17) neurons (7 mice/genotype, p>0.05, unpaired t tests). B) CCh-evoked medium duration afterdepolarization (ADP) measured 100ms post 1s-long stimulus (WT n=13, HOM n=21; p=0.07 TW ANOVA; *p<0.05 Fisher's LSD). C) Spike attenuation in control (dotted lines) and upon CCh-induced depolarization (markers) shown as ratio between last and first spike amplitude in 1s train (WT n=13, HOM n=19, TW ANOVA; *p<0.05 Fisher's LSD). D) Medium and slow duration afterhyperpolarizations (AHPs) quantified at the peak and 500ms post stimulus, respectively (inset). AHPs evoked at -65mV by a 100Hz burst of somatic current injections were equal in WT (13) and HOM S15A (18-19) mice (mAHP, -1.5 *vs* -1.2mV; sAHP, -0.2 *vs* -0.3mV, p>0.05, unpaired t test). CCh suppression of burst-evoked AHPs (**p<0.01 paired t tests) was

823 unchanged between genotypes (mAHP ~Δ1.5mV, sAHP ~ Δ 1mV, p>0.05 unpaired t test). E)
824 Example traces of isolated small-conductance Ca^{2+}-activated SK currents and full inhibition
825 by d-tubocurarine (dTC, grey). F) dTC-sensitive current amplitude (left) and charge (right)
826 were not different between groups (WT n=8, HOM n=10 cells, 4 mice/genotype, p>0.05
827 unpaired t tests). G) Example traces of spontaneous excitatory postsynaptic currents in WT
828 and HOMS15A mice H) Distribution of measured sEPSC properties for each genotype (WT:
829 1422-34 events, n=8 cells, HOM: 1455-65 events, n=7 cells; mean amp=14.0±0.8 *vs* 14.7±0.5
830 pA; instantaneous frequency=4.0±0.4 *vs* 4.3±0.3 Hz; N=3 mice/genotype; p>0.05, unpaired t
831 tests).

832

833

834

Figure S4

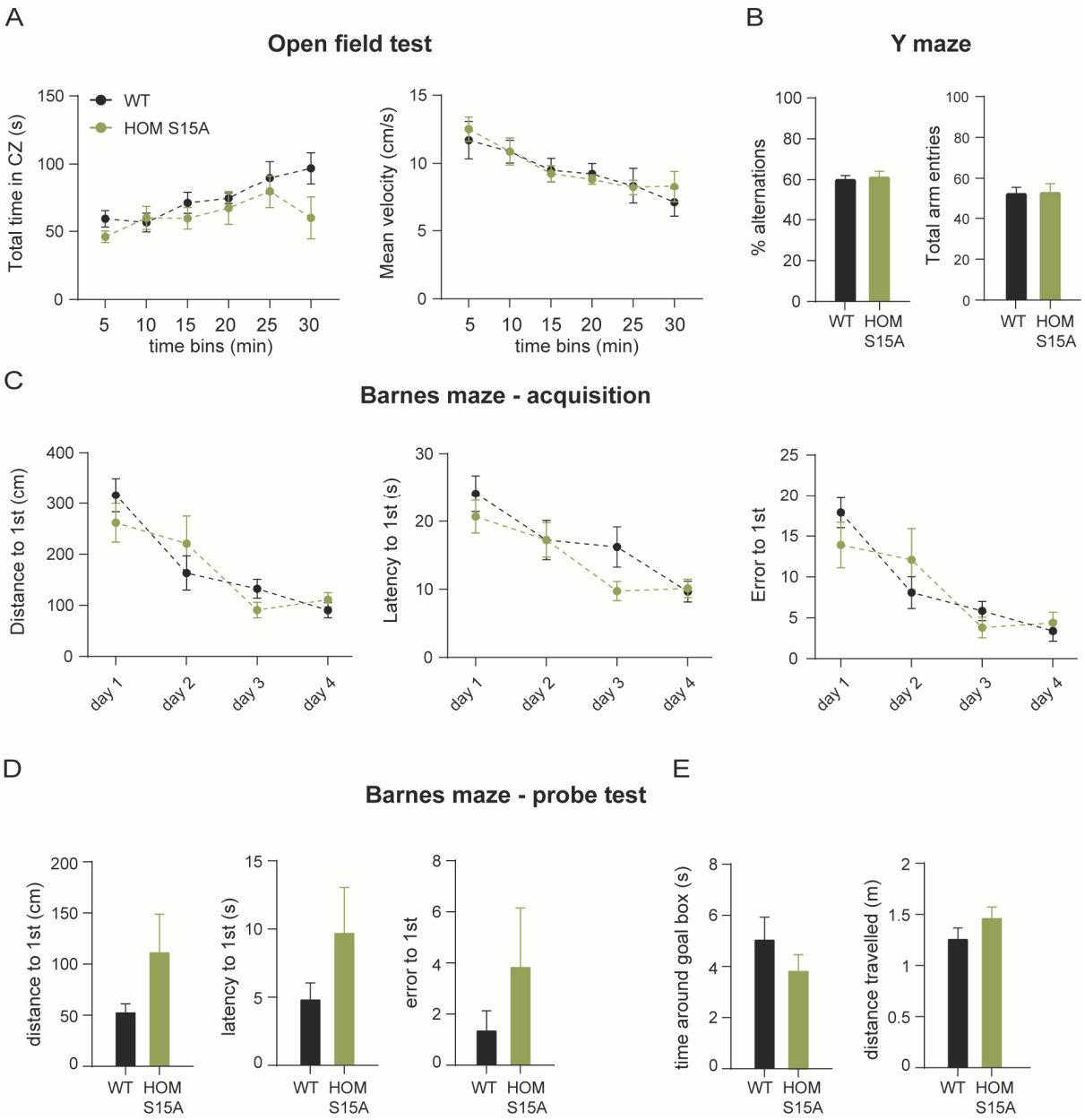

Figure S4. Behavioural characterization of Cav2.3 S15A phosphomutant mice. A) left: total time in the central zone (CZ) of the open field arena in WT (N=8) and HomS15A (N=7) mice (30 min test) ($p>0.05$, TW RM ANOVA; $p=0.08$ at 30 min, Fisher's LSD); right: mean displacement velocity ($p>0.05$, TW RM ANOVA). B) Percentage of successful spontaneous alternations (left) and total arm entries (right) in the Y-maze test show no deficits in arm recognition and exploration in phosphomutants ($p>0.05$, unpaired t test). C) Acquisition phase of the Barnes maze test with improved performance for both groups in the first 4 training days: distance travelled (left), latency (middle) and number of errors committed (right) during the 1st

visit to the escape box were not significantly different ($p>0.05$, TW RM ANOVA). D) memory assessment on probe day 5 compared using the same parameters as in C ($p>0.05$, unpaired t tests). E) Quantification of total time spent around the expected location of the goal box (left) and total distance travelled (right) ($p>0.05$ unpaired t tests).

871 ## Materials and Methods

872

873 ### Mouse handling and mutant generation

874 Animals were housed in a controlled environment with 12-hour light/dark cycle. They were fed
875 *ad libitum* and used in accordance with the principles of the "3Rs" and the Animals (Scientific
876 Procedures) Act 1986 of the United Kingdom. Protocols and procedures were approved by
877 institutional evaluations. With the exception of some *in vivo* experiments, mice were housed
878 in groups. Mouse strains were backcrossed into C57 Bl/6 (Jackson) and none of the
879 experimental mice were immunocompromised. Male and female mice aged embryonic day
880 (E)16.5 to postnatal 30 weeks were used as specified.

881 CDKL5 KO animals were a kind gift from Cornelius Gross [46]. Mutant Cav2.3 Ser15Ala animals
882 were created in-house using the CRISPR/Cas9 system. The guide contained the sequence
883 5'AGGCUCAGGCGAUGGAGACU3'. This replaced the original DNA sequence of 5'
884 AGGCGCAGGCGATGGAGACT 3' in CACNA1E. Genetically altered C57Bl6 embryos were
885 obtained using electroporation as part of Francis Crick Institute's Genetic Modification
886 Services. Genotype was determined by in-house PCR or Sanger sequencing (Source
887 Bioscience).

888

889 ### SILAC phosphoproteomics

890 Sample preparation

891 Mouse cortical neurons were cultured from individual male E16.5 embryos from a
892 heterozygous Cdkl5 female. Cdkl5 +/Y (WT) or -/Y (KO) genotype of embryos was determined
893 afterwards. Neurons were plated at a density of 8x10^6 cells per 10 cm dish coated with 60
894 µg/ml poly-D-lysine (Sigma) and 2.5 µg/ml laminin (Sigma). Cells were grown in neurobasal
895 media free of L-Arginine and L-Lysine (Invitrogen) supplied with either Lysine 8 (U-13C6, U-
896 15N2) and Arginine 10 (U-13C6, U-15N4) or Lysine 4 (4, 4, 5, 5-D4) and Arginine 6 (U-13C6).
897 L-Proline (200mg/ml) was supplemented to prevent Arginine to Proline conversion. At DIV4,
898 1 µM Ara-C was added to inhibit glia growth. For every embryo, one dish was labelled with
899 K8R10 (heavy) and one dish was labelled with K4R6 (light).

900 At DIV12, SILAC labelled primary neurons from 3 Cdkl5 WT and 3 Cdkl5 KO animals were
901 lysed in lysis buffer containing 20 mM Tris pH7.5, 100 mM NaCl, 10 mM $MgCl_2$, 0.25% IGEPAL
902 NP40, 0.5 mM DTT, 1x Protease Inhibitor Cocktail, 1 µM Okadaic Acid. Each sample was
903 checked for SILAC label incorporation and Arginine to Proline conversion. Lysates were mixed
904 to obtain 3x heavy WT/light KO and 3x heavy KO/light WT samples containing 1 mg total

905 protein. Proteins were digested overnight with Sequencing Grade Modified Trypsin/Lys-C
906 (Promega) at 37^{0}C, desalted using Sep-Pak Classic C18 Cartridges (Waters) and vacuum
907 dried completely. Samples were enriched for phosphopeptides using Titansphere titanium
908 dioxide beads (GL Science) in batch mode with the following buffers: Loading buffer: 80%
909 ACN, 5% TFA, 1M Glycolic Acid, Wash buffer 1: 80% ACN 1% TFA, Wash buffer 2: 10% ACN,
910 0.2% TFA, Elution buffer 1: 1% Ammonium Hydroxide, Elution buffer 2: 5% Ammonium
911 Hydroxide. Phosphopeptides were cleaned up using C18 Stage Tips with a centrifuge protocol
912 and vacuum dried completely. Samples were stored at -80^{0}C until required for analysis by
913 mass spectrometry.

914 Mass spectrometry

915 Each sample was resuspended in 35 µl 1% TFA, sonicated for 15 minutes and injected 3 times
916 (10 µl per injection). Peptide mixtures were separated on a 50 cm, 75 µm I.D. Pepmap column
917 over a 3 hr gradient and eluted directly into the mass spectrometer (Orbitrap Velos). Xcalibur
918 software was used to control data acquisition. The instrument ran in data dependent
919 acquisition mode with the top 10 most abundant peptides selected for MS/MS by CID, MSA
920 or HCD fragmentation techniques (one fragmentation technique per replicate).

921 Data processing was performed using the MaxQuant bioinformatics suite (v 1.3.0.5) and
922 protein database searching was done by the Andromeda search engine using a Uniprot
923 database of *Mus musculus* proteins amended with common contaminants. Default search
924 settings were used including an FDR of 1% on the phosphosite, peptide and protein level and
925 matching between runs for peptide identification. K4R6 and K8R10 were set as labels with a
926 maximum of 3 labeled AAs. Phosphorylation at serine, threonine or tyrosine residues,
927 oxidation (Met) and protein N-terminal acetylation were set as variable modifications.
928 Carbamidomethylation of Cys-residues was set as a fixed modification.

929 Data was further processed in Perseus v.1.6.15.0. Phospho (STY) sites from the six
930 experimental samples in the MaxQuant search were loaded and site tables expanded.
931 Potential contaminants and reversed hits were removed. Normalized H/L ratios were log2
932 transformed and filtered for rows containing at least three valid values. Potential CDKL5
933 substrates were annotated using the R-P-X-pS/pT motif [19]. A one-sample t-test was performed
934 comparing the normalized ratios to the null hypothesis and visualized as a volcano plot.

935

936 **Mutagenesis**

937 Point mutations were introduced using QuickChange site-directed mutagenesis (Agilent).
938 Complimentary primers contained the desired mutations flanked by at least 18 bp. To ensure
939 mutagenesis efficiency for each construct, two separate PCR reactions with each primer were

940 set up: 0.2 μM primer, 100 ng template DNA, 0.2 mM dNTP mix, 1x Pfu buffer and 2.5 U Pfu
941 Ultra HF. The PCR programme was run 4x, after which complementary samples were
942 combined and the PCR run repeated 20x. PCR products were treated with DpnI for 1hr at
943 37^0C and transformed into XL-10 Gold competent cells. At least 4 colonies were used for each
944 DNA miniprep (QIAprep, Qiagen) and mutations were confirmed by Sanger sequencing
945 (Source Bioscience). The constructs used were as follow: 1) HA-tagged human α1E subunit
946 (gene bank L27745.2, gift from L. Parent, Université de Montréal), in a commercial vector
947 under control of CMV promoter [92]. 2) The N-terminal FLAG-tagged full-length human $CDKL5_{107}$
948 and N-terminal HA-tagged human $CDKL5_{1-352}$ kinase domain construct kinase as previously
949 described [19].
950

951 **Cell line maintenance and transfection**

952 Tetracycline-inducible HEK293 cells expressing human Cavβ3 and α2δ1 subunits were
953 obtained from SB Drug Discovery (Glasgow, UK). HEK293 cells stably expressing human Cav
954 β1b and α2δ1 subunits were kindly provided by Andrew Powell (GSK Ltd., Middlesex, UK).
955 Naïve HEK293T cells were supplied by Francis Crick Institute's Cell Services.

956 All cells were cultured in high glucose DMEM with 10% Fetal Bovine Serum (tetracycline free,
957 Clontech or Gibco) and penicillin/streptomycin 50units/ml-50 mg/ml. They were passaged
958 using TrypLE Express and maintained under selection antibiotics as appropriate: HEKβ3/
959 α2δ1, Zeocin 300mg/ml (Invivogen) & Blasticidin 5mg/ml (Invivogen); HEKβ1b/α2δ1,
960 Puromycin 1mg/ml and Hygromycin-B 200mg/ml. Cell culture reagents were obtained from
961 Gibco/Invitrogen unless specified.

962 Selection antibiotics were removed before transfection and doxycycline 1μg/μl added in the
963 case of β3-expressing cells. Transient transfection was carried out using X-tremeGENE™ 9
964 reagent (Roche) following manufacturer's instructions. Total DNA was 1.5-1.6μg. For Western
965 blot experiments, human α1E-HA subunit and CDKL5 (HA-kinase domain or FLAG-full length)
966 were co-transfected in a 1:1 ratio, substituting kinase for empty pcdna3 vector in some cases.
967 For electrophysiological recordings α1E-HA, FLAG-CDKL5 full length and GFP (pcdna3) were
968 co-transfected at a ratio of 10:4:1 (HEK β3 cell line) or 8:4:1 (HEKβ1b cell line). To study
969 muscarinic regulation, human α1E-HA, FLAG-CDKL5, muscarinic receptor type 3/1
970 (CHRM3/1, Addgene) and GFP were co-expressed at a ratio of 8:4:3:1. For dopamine
971 modulation experiments, human α1E-HA, FLAG-CDKL5 and dopamine D2 receptor (gfp-
972 DRD2, Addgene) were co-transfected at a ratio of 2:0.75:1.

973

974

975 **Western Blotting**

976 Three different types of sample were used for Western blot experiments: 1) HEK293 cells 48
977 hr post-transfection, 2) Mouse brain tissue collected after cervical dislocation, followed by
978 dissection and snap-freezing in liquid nitrogen, 3) Human iPSC derived neurons obtained as
979 frozen pellets from Cleber Trujillo (UCSD, USA). Protocols for iPSC generation, patient *CDKL5*
980 mutations and related control details are described in [81]. All lysates were prepared in 1x/2x
981 sample buffer (Invitrogen) with 0.1-0.2 M dithiothreitol (Sigma). This was followed by
982 sonication, centrifugation at 13000g and denaturation at 70^0C, 10 min. Protein was loaded
983 onto NuPAGE 8% Bis-Tris polyacrylamide gels (Invitrogen) for electrophoresis and
984 subsequently transferred to polyvinylidene difluoride membranes (Millipore) for 15-22 hr at
985 20V in 10% MetOH, Tris Glycine buffer. Membranes were blocked for 30 min in 5-10%
986 skimmed milk and incubated with primary antibodies overnight at 4^0C or 1hr at room
987 temperature (RT). Secondary incubation in horseradish peroxidase-conjugated (HRP)
988 antibodies was for 1hr at RT. Chemiluminescence signals were detected using Amersham
989 ECL (Cytiva) and Amersham Imager (GE Healthcare). Analysis was perfomed using Fiji 2.1.
990 Phospho-S14/15 channel levels were measured as the ratio between pS14/15 Cav2.3 signal
991 and total Cav2.3 signal. Total channel levels are expressed as the ratio over loading control
992 GAPDH. Each replicate in a blot constitutes a data point normalized to the average internal
993 control signal in each blot. At least two independent immunoblot experiments with technical
994 replicates were used for quantification, as specified in figure legends.

995 Primary antibodies used in each sample were: mouse anti-HA 1:2000 (Biolegend, 901513;
996 HEK293), rabbit anti Cav2.3 N-terminus 1:250 (Covalab, custom 1, HEK293 & brain), rabbit
997 anti pS15 Cav2.3 1:500 (Covalab, custom 2, HEK293, brain & human neurons), mouse anti
998 Cav α1E 1:1000 (Synaptic Systems, 152411, human neurons), rabbit anti CDKL5 1:2000
999 (Atlas, HPA002847, HEK293), mouse anti GAPDH 1:50000 (Abcam, ab8245, brain & human
1000 neurons). Custom made Cav2.3 Ser15 phosphospecific antibodies were raised by immunizing
1001 rabbits with peptide PRPG(pS)GDGDSDQSRNC. Phosphorylated Cav2.3 antibody was
1002 obtained after double purification. First, they were selected against non-phosphorylated
1003 peptide PRPGSGDGDSDQSRNC. This antibody is used as total Cav2.3 antibody (custom 1).
1004 Next the eluted fraction was purified again by binding to PRPG(pS)GDGDSDQSRNC -linked
1005 beads, obtaining pSer15 Cav2.3 (custom 2). Secondary antibodies used were: donkey anti
1006 rabbit HRP 1:10000 (Jackson, 711-035-152), donkey anti mouse HRP 1:10 000 (Jackson,
1007 715-035-151).

1008

1009 ***In vitro* electrophysiology**

1010 HEK293 cells

1011 Cells were split 24hr after transfection and replated on glass coverslips and allowed to recover
1012 overnight. Whole-cell patch clamp recordings in isolated cells were performed 48-72 hr post-
1013 transfection at room temperature. Transfected cells were identified by GFP fluorescence. Data
1014 were sampled at 20kHz and filtered at 1-2 kHz. Cells were continuously perfused (1ml/min)
1015 with extracellular solution containing (in mM): NaCl 120, TEACl 20, HEPES 10, glucose 10,
1016 KCl 5, $MgCl_2$ 1, $CaCl_2$ or $BaCl_2$ 5, pH 7.4 with NaOH. Pipettes (2.5-3.5 ΩM) were pulled from
1017 borosilicate glass (1.2x0.69mm, Harvard Bioscience) and filled with the following intracellular
1018 solutions adapted from [38] to minimize current run-down (in mM): CsMeS 140, EGTA 5, $MgCl_2$
1019 0.5, MgATP 5, HEPES 10, for GPCR experiments; CsMethanesulfonate 125, TEACl 5, EGTA
1020 5, MgATP 5, Na_3GTP 0.3, Na-phosphocreatine 5, Na-pyruvate 2.5, HEPES 10, pH 7.25, 285-
1021 295 mOsm, all other recordings. Upon seal break, currents were evoked every 5/10s with a
1022 step from -80/-100mV (holding potential, HP) to 0/+10mV. After an initial run-up period, steady
1023 state current voltage (IV) relationships were obtained with 100ms depolarising test steps to
1024 +60/+80 in 10mV increments every 10s. For voltage dependence of inactivation the protocol
1025 consisted of a 1s pulse from -140 to +20mV in 10 mV increments, followed by a 50 ms test
1026 pulse to 0 mV, every 10s. Peak currents (I_{peak}) in response to test voltages (V_{test}) were used
1027 to plot IVs and measure the voltage dependence of activation and inactivation. Reversal
1028 voltage (E_{rev}) was estimated by extrapolating a linear fit to the IV curve from +20-+40 mV.
1029 Conductance (g) was calculated using the equation ($g=(I_{peak})/(V_{test}-E_{rev})$). Voltage of half-
1030 maximal activation or inactivation ($V_{1/2}$) were measured by fitting with a Boltzmann equation
1031 ($Y= A+(B-A)/(1+\exp((V-V_{1/2})/K))$ where Y is the conductance or the current, and A and B are
1032 the minimum and maximum amplitudes of the fit. Time course of open state inactivation (τ_{inact})
1033 was estimated by fitting a single exponential function to current decay in response to test
1034 pulses. The average of 3 fits at each voltage was used. For all transfection conditions, cells
1035 with outward currents >40% of the peak current at +10mV or with τ_{inact} that did not decay
1036 uniformly with depolarization were excluded from analysis. Similarly, cells were not used for
1037 current density or τ_{inact} comparisons if run-down was >30% of the maximal current recorded in
1038 the experiment as this is known to affect inactivation time [38]. To examine recovery from
1039 inactivation, an inactivating pulse to +10mV of 0.8-1s (pulse 1), was followed by a variable
1040 recovery period (Δ 150-200ms) and a test pulse to +10mV (pulse 2), at 0.1-0.3 Hz. Time
1041 course of recovery was calculated using the ratio of I_{peak} in response to pulse 2/pulse 1 plotted
1042 against duration of recovery period and fitted with single exponential equation. Carbachol,
1043 quinpirole and PMA were bath at ~3 ml/min whilst activating Cav2.3 currents with brief
1044 monitoring (25ms) test steps to 0 or +10mV, every 2, 5 or 10s, depending on speed of run-
1045 down. Upon steady state, IVs were obtained. Cells included in the analysis showed no
1046 significant changes in series resistance and a consistent shift in activation $V_{1/2}$, with current
1047 amplitude matching between IV and brief monitoring steps. Leak and capacitance subtraction

1048 was applied to all recordings using -P/5 protocol and series resistance compensated from 75-
1049 95% to keep voltage error <5mV.

1050

1051 ***Ex vivo* electrophysiology**

1052 Hippocampal slices

1053 Mice older than P10 were anaesthetized by intraperitoneal injection of ketamine (80mg/kg)
1054 and xylazine (10mg/kg). To avoid bias, the genotype was unknown at the time of experiment.
1055 Animals were decapitated and the brain transferred to ice cold artificial cerebrospinal fluid
1056 (standard aCSF) containing (in mM): NaCl 125, NaH_2PO_4 1.25, $NaHCO_3$ 26, KCl 2.5, glucose
1057 25, $MgCl_2$ 1, $CaCl_2$ 1, saturated with carbogen. Cerebellum and olfactory bulb were discarded.
1058 Coronal or transverse hippocampal slices (300µm) were prepared with a Leica VTS 1200S
1059 vibratome and transferred to an immersion storage chamber containing bubbled aCSF at 35^0C
1060 for 30 min. Slices were allowed to recover for a further 30 min at room temperature (RT) before
1061 electrophysiology experiments. Somatic whole-cell patch clamp recordings were obtained
1062 from CA1 pyramidal neurons using borosilicate electrodes (3-4.5 MΩ). Series resistance (R_s)
1063 and input resistance (R_{in}) were monitored throughout recordings using a 100ms, -5mV step
1064 from -60mV to evoke passive membrane responses. R_s was calculated from the amplitude of
1065 the capacitive transient and R_{in} from the steady state currents. These were sampled at 20kHz
1066 and filtered at 10kHz. The maximum change in Rs permitted was 25%.

1067 *R-type Ca^{2+} currents* - Recordings were obtained from young neurons (P10-11) no longer than
1068 6h post slicing using the blind technique. Currents were recorded at RT from P10-11 coronal
1069 slices during bath application of a modified aCSF solution (in mM): NaCl 115, TEACl 10,
1070 $NaHCO_3$ 26, KCl 2.5, NaH_2PO_4 1.25, glucose 25, $MgCl_2$ 1, $CaCl_2$ 2; and in presence of the
1071 following inhibitors (in µM): TTX 0.5, gabazine 1, APV 25, NBQX 5, 4AP 5, Nifedipine 10
1072 (Tocris), w-conotoxin GVIA 2, w-agatoxin IVA 0.2, w-conotoxin MVIIC 2 (Alomone) and BSA
1073 1mg/ml. Drug stock solutions were prepared in water and stored at -20^0C. External solution
1074 was constantly bubbled and re-circulated. Slices were exposed to ion channel inhibitors for at
1075 least 20 min before voltage clamp acquisition. Patch pipettes were filled with (in mM):
1076 CsMethanesulfonate 130, TEACl 10, Na-phosphocreatine 5, $MgATP_2$ 4, Na_3GTP 0.3, HEPES
1077 10, EGTA 2 and biocytin 0.2% pH 7.3 with CsOH. After 10 min stabilization in the whole-cell
1078 configuration, IV curves were obtained with voltage steps from -80 to +40, HP=-70mV. A -P/5
1079 leak and capacitance subtraction protocol was used and R_s was compensated 65-85%, to
1080 minimize voltage error. Capacitance (C_m) was calculated using equation: C_m [pF] = τ_m
1081 [ms]/R_s[MΩ], where τ_m is the decay time constant of capacitative transients. Time course of
1082 open state inactivation was estimated by iterative single exponential fit to current decay. A
1083 positive correlation was found between τ_{inact} and C_m for C_m<80pF, thus this was established as

1084 the cut off cell size criteria for inclusion in τ_{inact} comparisons. Cells with large cells outward
1085 currents at depolarising voltages (>50% of the peak current at +10mV) were also excluded.

1086 *Small-conductance Ca^{2+}-activated (SK) currents and excitatory postsynaptic currents (EPSC)*-
1087 Recordings were obtained from adult neurons (5-6 weeks) in transverse slices. SK currents
1088 were measured as tail currents following a 100ms step from -50 mV to +10mV (0.3 Hz) to
1089 engage VGCCs. Standard aCSF ($CaCl_2$ 2mM, RT) was supplemented with (in μM): TTX 0.5,
1090 TEA 1000 and XE991 5, to isolate SK currents by inhibiting temporally overlapping voltage-
1091 gated Na^+ and K^+ conductances. The intracellular solution was (in mM): KGluconate 135, KCl
1092 10, Na-phosphocreatine 10, $MgATP_2$ 2, Na_3GTP 0.3, HEPES 10, pH 7.3, supplemented with
1093 8-cloro-phenylthio cAMP 50μM, to inhibit the slow afterhyperpolarizing current. SK current
1094 identity was confirmed at the end of all experiments by reversible d-tubocurarine (dTC, 50μM)
1095 inhibition. dTC-subtracted currents were used for quantification. Traces were sampled at 5
1096 kHz and filtered at 1kHz. SK current amplitude was measured at the peak of the after-current
1097 and charge as the integral 500ms post stimulus. EPSCs were isolated at -70 mV in standard
1098 aCSF (1) ($CaCl_2$ 2.5mM, 30-32^{0}C) with gabazine 1 μM and Kgluconate-based internal solution.
1099 Traces were sampled at 10kHz and filtered at 2kHz. Upon 5 min stabilization in whole-cell, a
1100 2 min gap free trace was analysed using template-based event detection and threshold match
1101 >3.

1102 *Current clamp recordings* - Recordings were obtained from adult neurons (5-6 weeks) in
1103 coronal slices in standard aCSF (2mM Ca^{2+}, 30-32^{0}C) and Kgluconate-based internal solution.
1104 Membrane potential (V_{rest}) was measured throughout the recording with 0 current injection and
1105 maintained around -65mV during stimulation. Input-output relationships were obtained with 1s
1106 current injections from -100 to 450 pA in 50 pA increments. Traces were sampled at 10kHz
1107 and filtered at 5kHz. Action potentials were identified with threshold-based event detection
1108 (0mV) and amplitude measured from V_{rest}. Spike attenuation during the train was calculated
1109 as ratio between last and first spike amplitudes. Depolarizing plateau potentials (DPPs) were
1110 defined as sustained depolarizations >20mV upon stimulus termination. Medium duration
1111 afterdepolarizations (ADPs) were measured 100ms post-1s step depolarization. Firing
1112 patterns were compared using binomial tests or comparisons of non-linear least squares
1113 regression fits to the data distribution. The effect of carbachol on the medium and slow
1114 afterhyperpolarizations (mAHP and sAHP) was used as positive control for muscarinic
1115 receptor activation. AHPs were evoked at -65mV by a burst of five 2nA, 2ms somatic current
1116 injections at 100Hz every 20s and measured at the peak and 500ms post stimulus
1117 respectively.

1118 All patch clamp data was obtained with Multiclamp 700B, Digidata 1440A and pClamp™ 10
1119 software (Molecular Devices). Data were analysed using Clampfit 10.7/11.2 and OriginPro
1120 9.8. Liquid junction potential was not corrected. Statistical analysis was performed in

1121 GraphPad Prism 9. Student's T tests and one- or two-way ANOVA (TW ANOVA) with Geisser-
1122 Greenhouse correction followed by Fisher's LSD test were used for most statistical
1123 comparisons. Repeated measures (RM) ANOVA was used as appropriate if there were no
1124 missing values. Data are presented as mean ± S.E.M. Box and whiskers (min to max) or violin
1125 plots are used to illustrate data spread and frequency distribution respectively; percentile
1126 25/75, median and mean are indicated by lines/markers.

1127

1128 ***In vivo* electrophysiology**

1129 Chronic electrocorticogram recordings

1130 Surgical procedures were performed in adult male and female mice (8-10 weeks old) using a
1131 stereotaxic frame (Kopf) under isoflurane anaesthesia and temperature control. Each animal
1132 was subcutaneously implanted with an electrocorticogram (ECoG) transmitter (A3022B-CC-
1133 B45-B, Open Source Instruments, Inc.). The recording electrode was placed above the visual
1134 cortex (AP -2, ML 1.5) and the ground electrode in the contralateral prefrontal hemisphere (AP
1135 1.8, ML 1.5). Implanted WT and Hom S15A animals (total 18) were housed individually and
1136 no drug treatment was given. The ECoG was recorded wirelessly (sampling frequency 512
1137 Hz, band-pass filter 1-160 Hz) for two weeks using software from Open Source Instruments,
1138 Inc. Simultaneous video recordings were obtained (6x/hour) using IP cameras from
1139 Microseven (https://www.microseven.com/index.html). The coastline, kurtosis and power
1140 spectrum analysis (1-160Hz) were performed using Python. Researchers were blinded to
1141 animal genotype during data acquisition and analysis.

1142 Kainic acid susceptibility

1143 At the end of the chronic recordings, low dose 5mg/kg kainic acid (Tocris Bioscience)
1144 dissolved in sterile saline was administrated intraperitoneally every 30 minutes to assess brain
1145 susceptibility to increasing dosage of chemo convulsant. The clock started at the first injection
1146 from 0 minute. Seizure severity was initially assessed while the experiment was ongoing at
1147 10-minute intervals, using a modified Racine scale: 1. immobility; 2, hunched position with
1148 facial jerks, 3. rearing and forelimb clonus, 4. persistent rearing and forelimb clonus, falling, 5.
1149 generalized tonic clonic convulsions, or wild jumping [76]. These assessments were confirmed
1150 by re-analyzing the video recordings. Latency measures the length of time from the start of
1151 the experiment to the first indication of generalized seizure (Stage 5 on Racine scale). Both
1152 kainic acid inductions and analysis were performed by a researcher blinded to the genotypes.
1153 A total of 17 implanted mice were used for susceptibility experiments, one male mouse was
1154 removed from the study due to surgical complications with the transmitter. In a subset of these
1155 where transmitter performance was not compromised, ECoG recordings during seizure

1156 inductions were recovered and used for quantification. Traces were analysed using semi-
1157 automated seizure detection as described previously [75]. The cumulative coastline was
1158 calculated from when the first epileptiform activity was detected until the mice reached
1159 generalized seizure (stage 5).

1160

1161 **Behavioural analysis**

1162 Home Cage monitoring

1163 Two separate cohorts of WT and homozygous S15A Cav2.3 mice of both sexes and aged
1164 between 12-16 weeks were used. Animals were housed individually and monitored using the
1165 Digital Ventilated Cage system (DVC®,Techniplast, Italy). The DVC consists of standard size,
1166 barcoded IVC units equipped with a 3x4 arrangement of cage-floor electrodes. Capacitance
1167 sensing-based detection of animal position allows for real-time tracking of locomotion activity
1168 24/7. Following a 2-week-acclimatization period, baseline activity was recorded and analysed.
1169 Rotating wheels (Ø 4.4 in) were then introduced, and animals allowed to familiarize
1170 themselves for another week before data collection. All activity metrics were calculated using
1171 the DVC Analytics 3.4.0 platform [93]. For locomotion index, the average signal of all 12 cage
1172 electrodes was used. Data were grouped in 60 min bins for each day.

1173 Behaviour tests

1174 Behaviour experiments were conducted in 8-week-old WT and homozygous S15A Cav2.3
1175 littermates of both sexes, housed under an inverted light cycle. Mice were handled daily for
1176 one week prior to experiments. All tests were video recorded for off-line analysis. Tracking
1177 data were analysed using Ethovision XT 15 (Noldus Information Technology, Netherlands)
1178 equipped with three-point (nose, body centre, and tail) detection settings. One cohort of mice
1179 was used for all 7 tests, carried out in the order described below. Mice were allowed to
1180 habituate to the testing room for at least an hour before the behaviour test.

1181 Hind-Limb clasping – Mice were suspended by the middle of the tail and lifted 15 cm above
1182 the ground; the extent of hind-limb clasping was recorded for 15 seconds. The room lighting
1183 was kept at 90 Lux. Hind-limb clasping was scored from 0 to 3: score 0 = both hind limbs were
1184 splayed outward away from the abdomen; score 1 = one hind limb retracted inward toward the
1185 abdomen for at least 50% of the observation period; score 2 = both hind limbs partially
1186 retracted inward toward the abdomen for at least 50% of the observation period; score 3 =
1187 both hind limbs completely retracted inward toward the abdomen for at least 50% of the
1188 observation period. Hind-limb extension reflex severity scores were calculated by averaging
1189 three trials separated by 1 min.

Open field test - The apparatus consisted of an illuminated (70 lux) white floor PVC foam arena (50 x 50 x 40 cm). A central zone (16 x 16 cm) was pre-defined. Test mice were placed in the centre of the open field and allowed to explore the arena for 30 minutes. At the end of each trial, the mouse was returned to the home cage and the arena was cleaned. Total distance travelled in 30 minutes and percentage of time spent in the central zone were used as measures of locomotor activity and anxiety levels, respectively.

Accelerating Rotarod test - Day 1: Mice walked on a rotating rod (Ugo Basile model 47650, Italy) at constant speed (4 rpm) for three minutes for two acclimatization trials. Day 2: Each mouse was placed on the rotating rod for three test trials, during which the rotation speed gradually increased from 4 to 40 rpm within four minutes. The inter trial interval was 1 hr. Performance was evaluated by measuring the latency to fall.

Three-chamber social interaction test – The apparatus consisted of a white rectangular PVC foam arena (62x42x23 cm) divided into one central and two adjacent compartments of equal size compartments connected by square openings. Empty cylindrical wire cages (Ø 8 cm, height 18 cm) were placed in the lateral chambers. Each mouse was placed in the central chamber and allowed to explore the arena for 10 min. The brightness of the room was kept at 10 lux. Chamber occupancy during habituation was equal between groups. After this, the mouse was returned to the waiting cage for 3 minutes. To assess social preference, an unfamiliar WT mouse of the same age, sex and strain (stranger 1) was gently introduced inside one of the wire cages to serve as a social stimulus. An unfamiliar and inanimate object was added to the other wire cage as the non-social stimulus. The test mouse was placed in the apparatus containing the social and non-social stimuli for 10 minutes. After that, the test mouse was removed and kept in the waiting cage for 3 minutes. All compartments were cleaned with 30% ethanol solution before the next test phase. To assess preference for social novelty, the non-social object from the previous test phase was replaced by an unfamiliar mouse (stranger 2) and the previous stranger 1 (now familiar mouse) was placed into the wire cage of the opposite compartment. The test mouse was placed in the central chamber and allowed to explore the arena for the next 10 minutes, after which it was returned to the home cage. The location of the novel and familiar mice with respect to the side compartments was counterbalanced across trials. The exploration of the target mouse/object was scored when the mouse's nose was detected within 2 cm from the cylindrical wire cage.

Y-maze spontaneous alternation test – Testing occurs in a Y-shaped maze with three arms (1,2,3) made of opaque plastic (34 x 9 x 14 cm) oriented in a 120^0 angle. Each mouse was randomly placed into one arm and allowed to explore the maze for 10 minutes. Room lighting was kept at 10 lux. An arm entry was recorded manually when the mouse moved beyond the central triangle of the maze and entered an arm with all four paws. Alternation behaviour was defined as consecutive entries into each of the three arms in overlapping triplet sets (e.g.: 1,

2, 3 or 2, 1, 3 or 3, 2, 1). The percentage of alternations was calculated as the number of actual alternations divided by the maximum possible number of arm entries.

Barnes-maze test – Twenty-four hours before training, the animal was habituated to the apparatus and escape box for a minute. During the training phase (4 days), mice were trained to locate the target hole (with an escape chamber underneath) from among 20 holes evenly spaced around the perimeter of an elevated circular open field (Ø 96 cm). Each animal was initially placed in the centre of the arena covered by an opaque cylinder, which was removed 10-20s after the start of the trial. Room lighting was kept at 635 lux. The mouse is then free to explore the platform for 3 minutes using four visual cues to aid navigation. If the mouse does not enter the escape chamber within 3 minutes the experimenter guides the mouse gently to the escape box (20x11x7cm) and leaves the mouse inside for 1 min. This step is repeated two more times a day (3 trials in total per day) with at least 20 minutes in between where the mouse is placed back in its home cage. To assess learning, a probe test in carried out 24h after the last training, where the escape box has been removed from the target hole. The mouse is placed on the platform and free to explore it for 3 minutes. Distance to first: distance walked from the centre of the arena to the target hole (centre-point detection); latency to first: time to reach the target hole from the centre of the arena (centre-point detection); errors to first are defined as checking any hole before reaching the escape box (nose-point detection).

Contextual fear conditioning – The fear conditioning chamber (27x27x35 cm, Ugo Basile, Italy) was equipped with a shock grid floor and a digital Near Infrared Red Video Fear Conditioning system. Mice from each genotype and sex were examined in four successive phases comprising: conditioned acquisition (day 1), memory of the conditioned background context A (day 2), exploration in new background context B (day 3) and memory extinction in the conditioned context A (day 4-7).

Context A was characterized by a cubic shape, illuminated at 100 Lux and the presence of a vanilla odour. The floor consisted of metal rods, mediating the foot shock. Context B was also cubic shaped, not illuminated and without additional odour cues. On day 1: Mice were introduced in the conditioning chambers scented with vanilla odour for 8 min and received 3 unconditioned stimuli (US: 1s, 0.25 mA foot shock, 2 min inter-trials interval). To examine the conditioned response to the context, mice were reintroduced in the training context 24 h later (day 2) and monitored for 5 minutes in the absence of the US. On day 3, the mice were introduced to a new context (context B) for 5 min to examine whether freezing behaviour is associated to a specific context (context A). During days 4-7 mice were placed back in context A without US to assess extinction of the association of the specific context A and the US (which is described as a form of new learning).